

Article published :

<https://doi.org/10.1073/pnas.2316498121>

Main Manuscript for

Tailoring chemical bonds to design unconventional glasses.

Jean-Yves Raty¹, Christophe Bichara², Carl-Friedrich Schön³, Carlo Gatti^{4,5} & Matthias Wuttig^{3,6}.

¹ Condensed Matter Simulation, B5, Université de Liège, B4000 Sart-Tilman, Belgium

² Aix-Marseille Univ, CNRS, CINaM, UMR7325, Marseille, France

³ Institute of Physics IA, RWTH Aachen University, 52074 Aachen, Germany

⁴ CNR-SCITEC, Istituto di Scienze e Tecnologie Chimiche “Giulio Natta”, sezione di via Golgi, via Golgi 19, Milano, 20133 Italy

⁵ Istituto Lombardo Accademia di Scienze e Lettere, via Brera 28, 20121 Milano, Italy

⁶ Peter-Grünberg-Institute (PGI 10), Forschungszentrum Jülich, 52428 Jülich, Germany.

*Matthias Wuttig

Email: wuttig@physik.rwth-aachen.de

Author Contributions: All authors contributed to discussion and writing of the manuscript. CFS, CB, CG and JYR performed the calculations.

Competing Interest Statement: The authors declare that they have no competing interests.

Classification: Physical Sciences / Applied Physical Sciences.

Keywords: quantum materials, glasses, metavalent bonding, phase-change materials, chalcogenides, structure – property relationship

Abstract

Glasses are commonly described as disordered counterparts of the corresponding crystals; both usually share the same short-range order, but glasses lack long-range order. Here a quantification of chemical bonding in a series of glasses and their corresponding crystals is performed, employing two quantum-chemical bonding descriptors, the number of electrons transferred and shared between adjacent atoms. For popular glasses like SiO_2 , GeSe_2 and GeSe , the quantum-chemical bonding descriptors of the glass and the corresponding crystal hardly differ. This explains why these glasses possess a similar short-range order as their crystals. Unconventional glasses, which differ significantly in their short-range order and optical properties from the corresponding crystals are only found in a distinct region of the map spanned by the two bonding descriptors. This region contains crystals of GeTe , Sb_2Te_3 and GeSb_2Te_4 , which employ metavalent bonding. Hence unconventional glasses are only obtained for solids, whose crystals employ these peculiar bonds.

Significance Statement

Glasses and the corresponding crystals usually share a similar local order and comparable properties. We explain these similarities by quantifying chemical bonding. These calculations for a series of glasses and their crystals using quantum chemical bonding descriptors (electrons transferred and shared between atoms) demonstrate that in common glasses like SiO_2 , GeSe_2 and GeSe , the quantum-chemical bonding descriptors of the glass and the corresponding crystal hardly differ. To the contrary, for crystals only found in a distinct region of the map, spanned by the two bonding descriptors, unconventional glasses are obtained, which differ in both local order and optical properties. This region contains crystals of GeTe , Sb_2Te_3 and GeSb_2Te_4 , which employ metavalent bonding. Hence, we can design unconventional glasses by identifying those crystals, which employ these peculiar bonds.

Introduction

Crystallization and vitrification are important processes to produce solids with tailored properties. Protein crystallization demonstrates which large efforts scientists have undertaken to unravel the atomic arrangement in protein molecules. Glasses, on the other hand, attract with their ability to be shaped at ease above the glass transition temperature. Hence, crystals and glasses are the two most important states of solid matter. Scientists have early on pondered about the differences in atomic arrangement and material properties between glasses and the corresponding crystals. The similarity of many properties of simple oxides between the glassy and crystalline phase led Zachariasen to state a very practical rule: the short-range order in the glass should be essentially the same as in the crystal, since 'the atoms are held together by the same forces'.¹ Today, we would possibly replace the word 'forces' by 'bonding mechanism'. Zachariasen continued by discussing some simple rules, which help to identify and predict those oxides that can easily form glasses.

Indeed, short range order has been measured in many glasses since that time and it was shown to be close (with minor distance and angular fluctuations and few coordination defects) to that of the corresponding crystal. Such glasses are also denoted as Zachariasen glasses or glassy covalent networks. Now, one can wonder whether it is possible to break this rule and design functional glasses that are unconventional in the sense that they do not bear the same short-range order and opto-electronic properties as their crystal. A first indication that this will be possible is given by Phase Change Materials (PCMs), which are utilized to store data² and realize active metasurfaces as well as nanophotonic switches³ and neuromorphic computers.⁴ In these, the atomic arrangement differs considerably between the glass-like (amorphous) material and the corresponding crystal.⁵⁻⁸ Furthermore, good phase change materials crystallize very quickly, a necessity to rapidly switch between the glassy/amorphous and crystalline state in memory applications.⁹⁻¹¹ Pronounced differences between the glass and the crystalline state are also observed for several characteristic properties such as the optical dielectric constant ϵ_∞ (a measure of the electronic polarizability), the Born effective charge Z^* (a measure of the chemical bond polarizability) or the effective coordination number (ECoN) (a measure of the atomic arrangement).¹² The difference in optical and electrical properties, in conjunction with the ability to switch rapidly between both states is responsible for a range of applications of phase change materials, including optical and electronic data storage, as well as photonic devices.^{3,13} Hence,

PCMs reveal the characteristic property portfolio of quantum materials, i.e. a distinct change of properties upon external stimuli.¹⁴

This raises the question which mechanism is responsible for the pronounced deviation of properties and the differences in atomic arrangement between the glass and the crystalline state. We will answer this question by employing recently developed concepts to analyze chemical bonding utilizing quantum-chemical tools.¹⁵⁻¹⁹ This will enable us to challenge Zachariasen's conjecture. Does the bonding in glassy compounds always correspond to their crystalline counterparts? At least for phase change materials we will present compelling evidence for the contrary. We will generalize that the functional nature of these unconventional glasses arises from rather unusual chemical bonding in the crystalline state.

Results and Discussion

Before quantifying the chemical bonding in glassy phase change materials, we will explore the bonding in glassy SiO₂, the prime example of a network forming glass already discussed by Zachariasen in 1932. To this end, Fig. 1A displays the number of electrons shared between adjacent atoms as a function of the interatomic spacing for SiO₂ in the crystal and in the glass. The number of electrons shared (ES) between adjacent atoms is twice the delocalization index (DI), the number of electron pairs formed between two atoms. This quantity is determined from the quantum

mechanical wavefunction, in particular from the non-classical part (the electron exchange contribution) of the electron pair density (see SI for more details).¹⁵

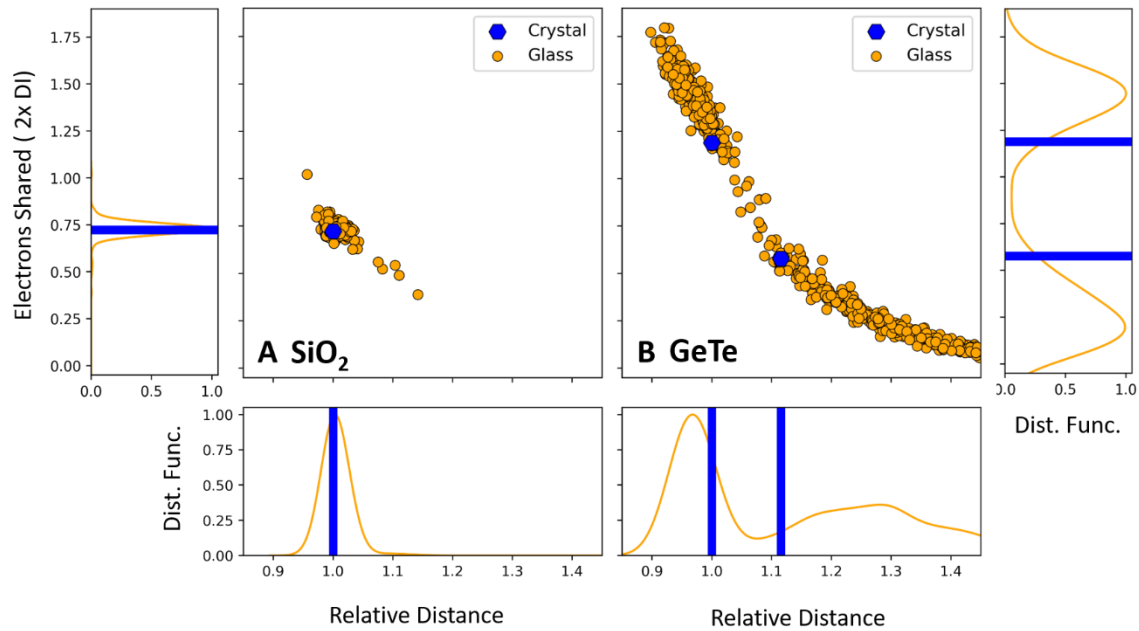


Fig. 1. Comparison of chemical bonding and atomic arrangement in glassy and crystalline SiO₂ (left) and GeTe (right). For SiO₂, the atomic arrangement in the crystal (indicated by bars) and the glass is very similar; the glass only shows a small variation in bond length (Zachariasen glass). Interestingly, the quantum chemical bonding descriptor, the number of electrons shared between adjacent atoms is very similar for both phases, too. This is fundamentally different for GeTe, where the distribution functions for both the Ge-Te distances as well as the number of electrons shared ($ES = 2 * DI$) between adjacent atoms differ significantly between the two phases. GeTe hence forms a non-Zachariasen glass. The relative distance is the interatomic distance divided by the first neighbor distance in the crystal.

Ionic bonds typically only share less than an electron ($ES < 1$), while standard 2 center – 2 electron (2c-2e) covalent bonds tend to share an electron pair, i.e. have an ES value close to 2. The ES value of SiO₂ is only 0.72, since each oxygen atom receives 0.8 electrons from two neighboring Si atoms, in agreement with the high polar character of the Si-O bond. Fig. 1A compares the atomic arrangement in crystalline and glassy SiO₂, analyzing more than 1000 bond distances in the latter. It confirms that the atomic arrangement in crystalline and glassy SiO₂ can be hardly distinguished (see Ref.²⁰), at least as far as the short-range order is concerned. Interestingly, Fig. 1A also shows the reason for this similarity. An analysis of the number of electrons shared between adjacent atoms shows an almost identical situation for glassy and crystalline SiO₂, i.e. the bonding in both phases

hardly differs. This corroborates the conjecture that oxide glasses like SiO_2 have the same short-range order as the crystal, since the chemical bonding is very similar. In GeTe, instead, a very different situation is encountered. The atomic arrangement in the glassy phase is characterized by a much larger difference between shorter and longer bonds and a wide distribution of atomic distances. This can be attributed to pronounced differences in chemical bonding, in striking contrast to a view expressed recently (²¹, see SI Appendix). Glassy GeTe hence forms a non-Zachariasen glass. It can be observed that, in any glass, when the distance (and chemical order) is equal to that of the crystal (see SI Appendix Fig. S1), the number of shared electrons is similar. In the particular case of GeTe, aligned bonds are longer (about 3\AA) than those in the crystal and share about 1 electron, indicative of 3c-2e bonding. As expected the electron sharing is decreasing with increasing atomic separation and decreasing covalent character of the bond. This quantifies the common belief that the bond length scales with the bond strength. A similar behavior was reported²¹ for a number of chemical-bonding indicator data, calculated at the bond critical points (BCPs) in simulated models of amorphous and crystalline GST. It is not surprise that the properties of bonds in amorphous and crystalline structures are similar when they are evaluated *at a common geometry*. This is merely a consequence of the local character of the properties being examined. Those properties considered in Ref. 21 are local in nature since they refer to a precise point, the BCP, taken as the most representative point along the bond path joining two adjacent nuclei. The DIs, despite being the result of an integration of the exchange correlation density over the two atomic basins of these atoms, are known to be also fundamentally local in character. It is therefore not surprising that the same (local) atomic arrangement in the glass and the crystal is accompanied by the same chemical bonding descriptors. This is the essence of the Zachariasen conjecture, the similarity of chemical bonding in the glass and the crystal leads to a similarity in atomic arrangement.

In the supplement, the comparison of the atomic arrangement and chemical bonding is presented for several solids. Some of them closely match SiO_2 , i.e. they show the same bonding descriptors and atomic arrangement as in the crystalline state. This holds for GeSe_2 but also to a good approximation for GeSe. Yet there are compounds where the glass and the crystal have significant differences in their atomic arrangement.⁵⁻⁸ Besides GeTe, this also holds for GeSb_2Te_4 ²² a prototypical phase change material and Sb_2Te_3 . Apparently, GeSb_2Te_4 , Sb_2Te_3 ²³ and GeTe form non-Zachariasen glasses (NZG), where the atomic arrangement and chemical bonding differs significantly between the glass and the crystal.

To quantify the departure from the Zachariasen conjecture in different glasses, we define a local order parameter based on the analysis of the local environment of each atom. To this end, configurations for the glass and the crystal are generated by DFT based Molecular Dynamics at

finite temperature (300 K). Hence, even in the crystal a distribution of atomic distances is found. We consider the distributions of the first N_b neighbors surrounding each atom, averaged for each species, as previously used in Ref.²⁴. These distributions overlap (Fig. 2A) and, for each species, their averages (Figs. 2B, 2C) can be used to define the order parameter NZ as the difference between the first neighbor distances in the crystal and the glass, properly weighted to treat all species on an equal footing (see SI Appendix).

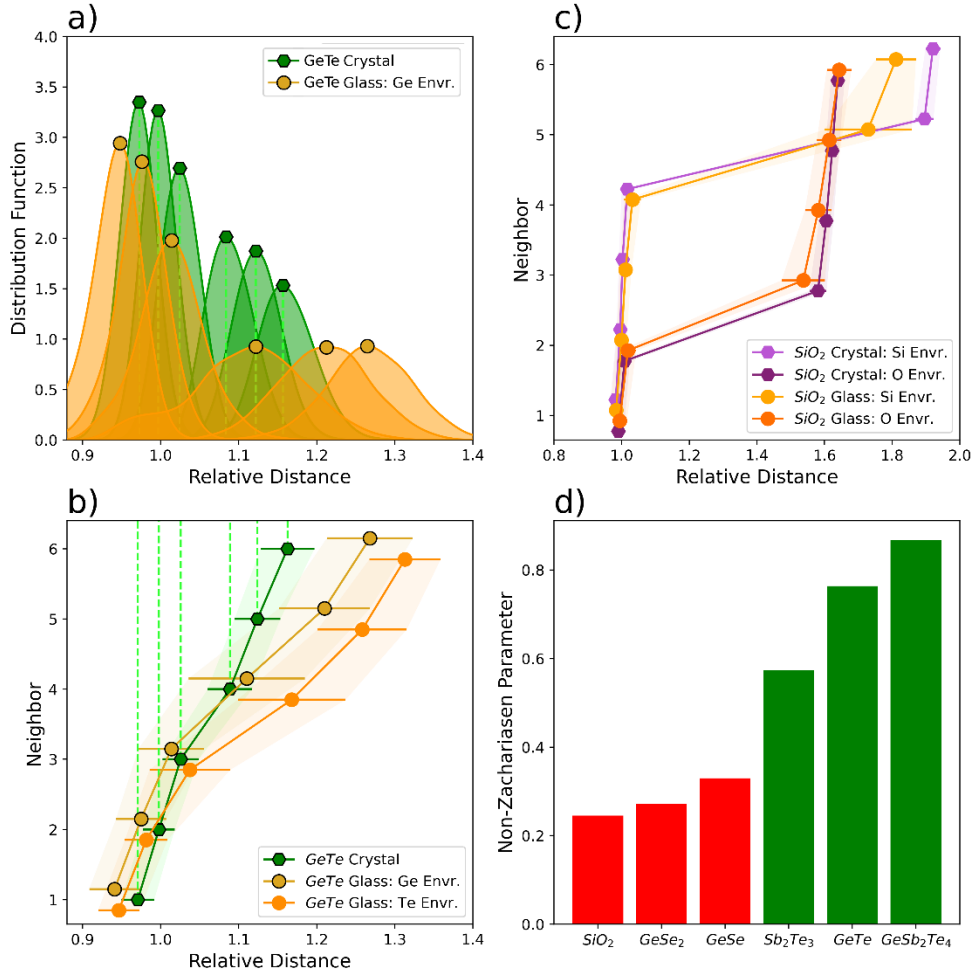


Fig.2 Comparison of the atomic arrangement in glassy and crystalline GeTe (left), SiO₂ and other glasses (right). a) Distributions of the six normalized distances between the first Ge neighbors of glassy (orange) and crystalline α -GeTe (green), from which the average distances (b) are calculated. b) Averaged, normalized first neighbor distances for crystalline and glassy GeTe (see Ref.²⁴). $d_0=2.86$ Å is the short GeTe neighbor distance in α -GeTe. There is only one (green) line for the crystal since Ge and Te atoms are equivalent. The atomic arrangement in glassy GeTe differs significantly from crystalline GeTe. Data for Ge and Te neighbors are shown since the

formation of a small number of tetrahedral Ge sites, caused by some homopolar bonds, leads to a small asymmetry of the distribution function. c) d_i/d_0 for crystalline and glassy SiO₂. $d_0=1.63$ Å is the Si-O distance. The local environments for the glass and the crystal are very similar. In panels b) and c) the error bars are the standard deviations of the distributions. d) Non Zachariasen (NZ) parameter measuring the difference between the local atomic arrangements in crystal and glasses for selected compounds. While GeTe, Sb₂Te₃, and GeSb₂Te₄ show pronounced differences between glass and crystal, only small differences for SiO₂, GeSe₂ and GeSe are found.

In crystalline SiO₂, (Fig. 2B), the first four distances around Si are equivalent, hence d_i are aligned, while the first six distances in crystalline GeTe displayed in Fig. 2A are not, revealing the slight Peierls distortion of the crystal at 300 K. In glassy GeTe, the much larger splitting of the distance distribution is a signature of a markedly different atomic arrangement around Ge and Te atoms. Comparing panels Fig.2 B C reveals that this difference, quantified by the NZ parameter, is large for GeTe and very small for SiO₂. As displayed in Fig. 2D, SiO₂ (0.25), GeSe₂ (0.27) and GeSe (0.33) have low NZ values because their local orders in crystalline and glassy states are very similar. On the contrary, the four GeTe structures tested, which differ by their decreasing amount of quasi-aligned bonds⁶, Sb₂Te₃ and the two GeSb₂Te₄ structures have significantly larger NZ values, in the 0.57-0.92 range. The local order in these glassy phase change materials structures is different from that of their crystalline counterpart. They are prototypes of NZG and their bonding mechanism, characterized using advanced quantum mechanical tools is also different.

The pronounced differences in the atomic arrangement between the different glasses and crystals compared in Fig. 2D raise the question, how the properties of both phases differ for the different solids (see SI Appendix Table S4 for all property values). This is depicted in Fig. 3 for six different properties including the optical dielectric constant ϵ_∞ , the effective coordination number (ECoN), the Born effective charge Z^* , the maximum height of the absorption peak ϵ_2^{Max} , and its energy $E(\epsilon_2^{Max})$, as well as the maximum vibration frequency ν_{max} . This last quantity hardly differs between the glass and the crystal for any of the materials studied. For the other quantities, especially those which are related to chemical bonding, like the optical properties and the chemical bond polarizability Z^* , some materials show striking differences between glass and crystal, while others do not. Fig. 3 reveals that only for those solids, where the atomic arrangement differs significantly

between the glassy and the crystalline phase, pronounced changes of properties accompany crystallization of the glassy phase.

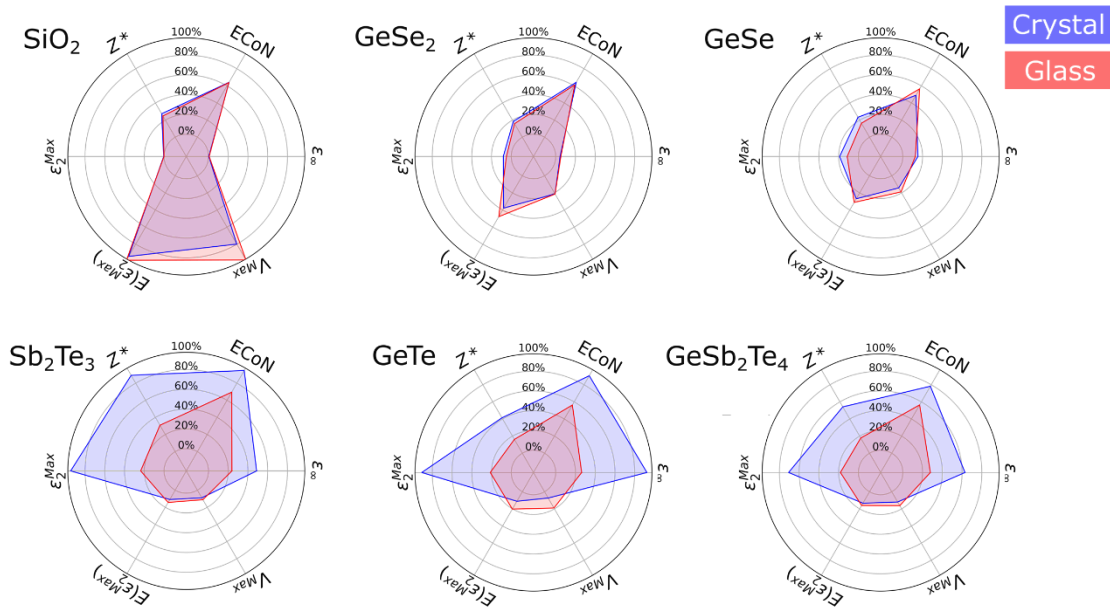


Fig. 3. Comparison of the properties of 6 different glasses (red) and their crystalline counterparts (blue). Six different quantities are depicted to show the differences between glass and crystal; the effective coordination number (ECoN), the optical dielectric constant ϵ^∞ , the maximum vibration frequency ν_{max} , the maximum height of the absorption peak ϵ_2^{max} , and its energy $E(\epsilon_2^{max})$, as well as the (cation) Born effective charge Z^* . Pronounced changes of properties upon crystallization are only observed for the three non-Zachariasen glasses Sb_2Te_3 , $GeTe$ and $GeSb_2Te_4$ (100% scale is $ECoN=6$, $\epsilon^\infty=80$, $\nu_{max}=40$ THz, $E(\epsilon_2^{max})=10$ eV, $\epsilon_2^{max}=100$ and $Z^*=12$ e).

Zachariasen has argued that the atomic arrangement in oxide glasses would be the same as in the corresponding crystal, since the chemical bonding is the same in both phases. This conjecture can now be verified with the quantum chemical bonding analysis already shown for $GeTe$ and SiO_2 in Fig. 1. All solids studied here have been depicted in the map displayed in Fig. 4. This map is spanned by two different quantum-chemical bonding descriptors, the number of electrons transferred and the number of electrons shared between adjacent atoms. The map separates different bonding mechanisms rather well. Ionic bonding is characterized by pronounced electron transfer between adjacent atoms, while in covalent bonding pronounced electron sharing (electron pair formation) prevails. The large number of nearest neighbors in metals leads to a small number of electrons shared between adjacent atoms. In conjunction with moderate charge transfer this locates solids which employ metallic bonding in the lower left corner of the map. Between covalent

and metallic bonding, another bonding mechanism is located, which is characterized by a characteristic property portfolio including large values of the Born effective charge Z^* , the optical dielectric constant ϵ_∞ . Solids which are characterized by these properties have been denoted as ‘metavalent’ solids or incipient metals.¹² Crystalline GeTe, Sb₂Te₃ and GeSb₂Te₄ fall into this category.

With the quantum chemical bonding descriptors one can now compare the glassy and crystalline phases of solids. This comparison shows that for all solids, where the atomic arrangement and properties of the glass and the crystal barely differ (SiO₂, GeSe and GeSe₂), the chemical bonding descriptors also hardly change. All of these glasses hence fulfil the Zachariassen conjecture, that the close similarity of atomic arrangement in both phases is due to the similarity in chemical bonding. Yet, there are also NZGs (GeTe, Sb₂Te₃ and GeSb₂Te₄). These are glasses, which are formed upon vitrification of incipient metals. Such metavalent crystals are characterized by a competition of electron delocalization (as in metallic bonding) and electron localization (as in covalent or ionic bonding). This leads to pronounced changes upon external stimuli, characterizing these solids as quantum materials.

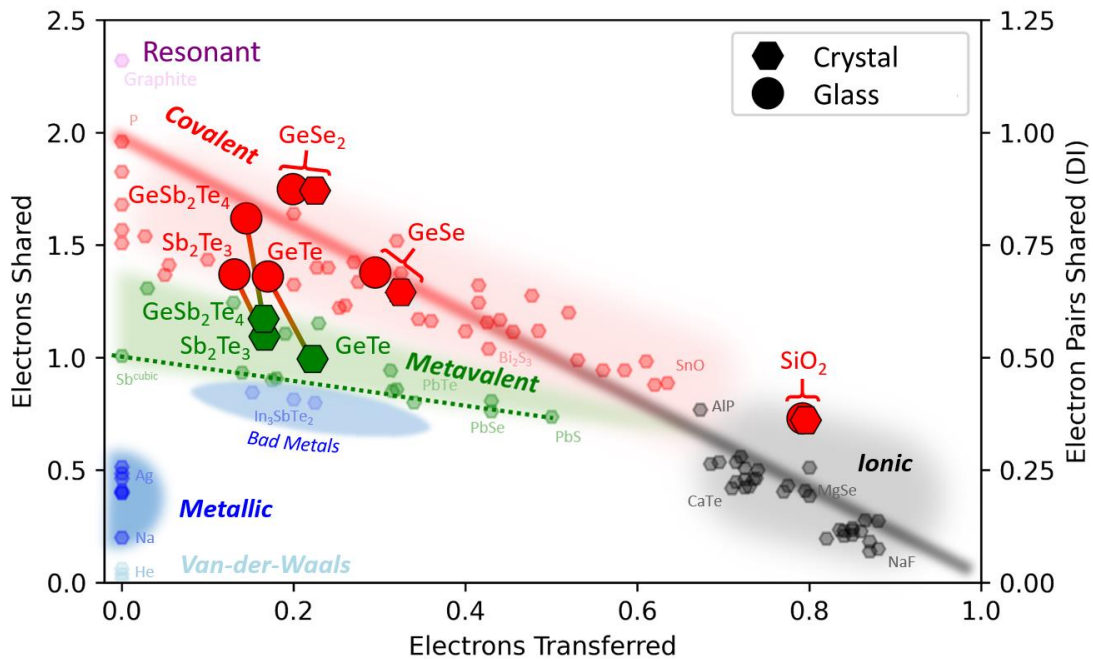


Fig. 4. 2D map classifying chemical bonding in crystals and glasses. The map is spanned by the number of electrons shared (*left y-axis*) between adjacent atoms and the electron transfer renormalized by the formal oxidation state (*a*). Different colors characterize different material properties and have been related to different types of bonds. The glasses of three solids are

characterized by a bonding mechanism which closely resembles the crystal (GeSe_2 , SiO_2 and GeSe). On the contrary, for GeTe , Sb_2Te_3 , and GeSb_2Te_4 , pronounced changes in bonding occur upon crystallization. While crystalline GeTe , Sb_2Te_3 , and GeSb_2Te_4 employ metavalent bonding, their glasses are covalently bonded. Metavalent crystals show characteristic features of quantum materials, i.e. they show a pronounced change of properties upon external stimuli like pressure or temperature. These materials change their bonding mechanism upon vitrification, while this is not the case for any other bonding mechanism in solids.

Glass formation in these chalcogenide-based quantum materials leads to pronounced changes of atomic arrangement, turning the bonding more covalent. Hence, only such materials which form metavalent crystalline solids, reveal a pronounced change of bonding upon crystallization. It is possibly no surprise that Zachariasen could not yet envision in 1932 the advent of such quantum materials and their unconventional property portfolio we witness today. The property changes of these materials upon crystallization are exploited in different applications such as phase change materials for optical and electronic data storage as well as neuromorphic computing. Fig. 4 reveals that metavalent solids are prime candidates as phase change materials since they offer the desired pronounced property contrast between the glassy and the crystalline phase. Yet, Fig. 4 offers additional insights. The quantum chemical bonding descriptors which span the map in this figure are also excellent property predictors. As shown recently, there is a close relationship between the position of the map and the resulting band gap as well as the dielectric function $\epsilon_2(\omega)$.¹⁹ It has even been demonstrated that the crystallization kinetics is closely related to the position of the map in the metavalent regime. Compounds closer to the green dashed line crystallize (switch) much more rapidly than metavalent solids which are located closer to the border between metavalent and covalent bonding.²⁵

At the same time, the findings presented here also lead to several interesting questions and should motivate relevant follow-up studies. First of all, it would be rewarding to increase the number of glasses that are depicted in Fig. 4. It could be for instance very interesting to further explore solids, whose crystals are located right above the upper edge of metavalent solids. In this region p-bonded compounds are found, such as Sb_2Se_3 or Sb_2S_3 , which offer larger band gaps than metavalent crystals, beneficial for photonic applications in the visible. The present design rule and the corresponding map can help to identify such photonic materials.

Finally, the most interesting questions seem related to the border between metavalent and metallic bonding. First studies have shown that there are even plasmonic phase change materials, i.e.

crystalline phases that have metallic-like (plasmonic) optical properties. In_3SbTe_2 is one of these materials, which has a glassy phase with a band gap of about 0.7 eV.²⁶ Hence, one can switch between a metallic-like crystalline phase and an infrared-transparent covalent glass, providing interesting application opportunities.²⁷ It seems very rewarding to look for additional plasmonic phase change materials at the border between metallic and metavalent bonding. Finally, one can ponder if there are any other crystalline metals which have unconventional phases when rapidly quenched from the melt. For instance, chiral metals like AlPt ²⁸ are potential candidates in this search for such unconventional non-crystalline phases. It will be interesting to locate such metals in Fig. 4, as well. The generality of the method makes it directly applicable to quantify the possible bonding origin of the changes observed in glassy MOF²⁹ and hybrid perovskites³⁰, for which metavalent bonding has been shown to prevail in a number of crystalline phases.³¹

To briefly conclude, we have shown that upon vitrification crystals with the peculiar metavalent bonding turn into glasses, leading to significant changes in terms of bonding, short-range order and opto-electronic properties. This finding provides a clear design rule, how to find unconventional glasses, i.e. those with opto-electronic properties which change significantly upon crystallization. Upon inversion of this argument, it is now also easy to understand why ordinary glasses have similar optical properties to their crystalline counterpart, since in these solids the bonding hardly changes during crystallization.

Materials and Methods

Six different glasses compositions (SiO_2 , GeSe , GeSe_2 , Sb_2Te_3 , GeSb_2Te_4 and GeTe) are studied using Density Functional Theory³² and molecular dynamics. Amorphous/glassy configurations with 189 to 249 atoms have been generated by melt-quench technique with VASP³³ using PBE exchange correlation functional³⁴ together with PAW potentials.^{35,36}

The systems are cooled down from 3000 K in several steps, first slightly above and below the experimental melting temperature, then by 100 degrees intervals down to 300 K. At each temperature plateau, the density is adjusted to obtain negligible residual stress.

For each system, the crystal was also simulated with MD at 300K with gamma point sampling and supercells counting 140 to 216 atoms. For GeTe , GeSb_2Te_4 and Sb_2Te_3 , further annealing and data acquisition at 300 K was performed using self-consistent DF2 van der Waals functional³⁷ and fixed volume, as in Ref.⁶.

The Born effective charge and static dielectric constant have been computed using Density Functional Perturbation Theory including local field effects³⁸ whereas the frequency dependent

imaginary dielectric function was computed using a sum over DFT states. Finally, the vibrational frequencies have been computed using finite differences on fully relaxed structures.

To quantify the impact of aging on bonding, we computed 4 different GeTe structures with different total energies (see Ref. ⁶) as well as two GeSb₂Te₄ models.

Computations

PAW SCF wave function calculations for all the systems for which LIs and DIs have been calculated were performed with the pw.x module of the Quantum Espresso (QE) package³⁹. The all-electron density is used to determine the QTAIM atomic basins by Critic2.^{40,41} PAW wave functions are then transformed into Maximally Localized Wannier Functions through the Wannier90 code.⁴² These are used by the Critic2 code to compute the localization and delocalization indices (DI and LI). The convergence of the final DI and LI values was checked on the crystal phases calculations.

Averaged DI using the Effective Coordination number ECON

To compute an average value for the number of electrons shared (twice the delocalization index), we weighted the DI contributions according to the EcoN definition.⁴³

This prevents the use of any distance cutoff to define the coordination number in the disordered system. In order to provide a direct comparison, the DI have been averaged in this same way for the crystalline phases. For crystalline GeTe, Sb₂Te₃ and GeSb₂Te₄, the ECON values (averaged over the species) equal 5.58, 5.84 and 4.45, respectively.

For any given atom *i*, an effective average interatomic distance r_{avg} is defined as:

$$r_{avg} = \frac{\sum_{j=1,N;j \neq i} r_{ij} e^{1-(r_{ij}/r_1)^6}}{\sum_{j=1,N;j \neq i} e^{1-(r_{ij}/r_1)^6}}.$$

r_{ij} being the interatomic distance between atom *i* and *j* and r_1 the shortest distance among these.

The effective coordination number and effective delocalization index are then obtained with

$$ECoN = \sum_{j=1,N;j \neq i} e^{1-(r_{ij}/r_{avg})^6}$$

$$DI_{avg} = \frac{1}{ECoN} \sum_{j=1, N; j \neq i} DI_{ij} e^{1-(r_{ij}/r_1)^6},$$

DI_{ij} being the delocalization index between the Bader basins of atoms i and j .

Acknowledgments

JYR and MW are grateful to Prof. Marco Bernasconi and Prof. Yuanzheng Yue for pre-refereeing the paper. JYR acknowledges computational resources provided by the CÉCI funded by the F.R.S.-FNRS under Grant No. 2.5020.11 and the Tier-1 supercomputer of the Fédération Wallonie-Bruxelles, infrastructure funded by the Walloon Region under grant agreement n°1117545. JYR acknowledges funding from the FRS-FNRS (CDR ABIGLO). Some of us (MW, CFS) acknowledge funding in part from the Deutsche Forschungsgemeinschaft (DFG) via the collaborative research center Nanoswitches (SFB 917) and in part from the Federal Ministry of Education and Research (BMBF, Germany) in the project 16ME0398K (NeuroTEC II)) as well as computational resources granted from RWTH Aachen University under project p0020357.

References

1. W.H. Zachariasen, The atomic arrangement in glass. *J. Am. Chem. Soc.* **54**, 3841–3851 (1932)
2. M. Wuttig, N. Yamada, Phase-change materials for rewriteable data storage. *Nature Mater.* **6**, 824-832 (2007)
3. Q. Wang *et al.*, Optically reconfigurable metasurfaces and photonic devices based on phase change materials. *Nat. Photon.* **10**, 60-65 (2016)
4. I. Boybat *et al.*, Neuromorphic computing with multi-memristive synapses. *Nat. Commun.* **9**, 2514 (2018)
5. A.V. Kolobov *et al.*, Understanding the phase-change mechanism of rewritable optical media. *Nat. Mater.* **3**, 703-708 (2004)
6. J.Y. Raty *et al.*, Aging mechanisms in amorphous phase-change materials. *Nat. commun.* **6**, 1-8 (2015)
7. S. Caravati, M. Bernasconi, T.D. Kühne, M. Krack, M. Parrinello, Coexistence of tetrahedral- and octahedral-like sites in amorphous phase change materials. *Appl. Phys. Lett.* **91**, 171906 (2007)
8. W. Zhang, R. Mazzarello, M. Wuttig, M. Ma, Designing crystallization in phase-change materials for universal memory and neuro-inspired computing. *Nat. Rev. Mater.* **4**, 150-168 (2019)
9. F. Rao *et al.*, Reducing the stochasticity of crystal nucleation to enable subnanosecond memory writing. *Science* **358**, 1423-1427 (2017).
10. D. Loke *et al.*, Breaking the speed limits of phase-change memory. *Science* **336**, 1566-1569 (2012)

11. G. Bruns *et al.*, Nanosecond switching in GeTe phase change memory cells. *Appl. Phys. Lett.*, **95**, 043108 (2009)
12. M. Wuttig, V.L. Deringer, X. Gonze, C. Bichara, J.Y. Raty, Incipient metals: functional materials with a unique bonding mechanism. *Adv. Mater.* **30**, 1803777 (2018)
13. M. Wuttig, H. Bhaskaran, T. Taubner, T. Phase-change materials for non-volatile photonic applications. *Nat. Photon.* **11**, 465–476 (2017)
14. D.N. Basov, R.D. Averitt, D. Hsieh, Towards properties on demand in quantum materials. *Nat. Mater.* **16**, 1077 (2017)
15. X. Fradera, M.A. Austen, R.W.F. Bader, The Lewis model and beyond. *J. Phys. Chem. A* **103**, 304-314 (1999)
16. P. Golub, A.I. Baranov, Domain overlap matrices from plane-wave-based methods of electronic structure calculation. *J. Chem Phys.* **145**, 154107 (2016)
17. A. Otero-de-la-Roza, A.P. Pendás, E.R. Johnson, Quantitative electron delocalization in solids from maximally localized Wannier functions. *J. Chem. Theory Comput.* **14**, 4699-4710 (2018)
18. J.Y. Raty *et al.*, A quantum-mechanical map for bonding and properties in solids, *Adv. Mater.* **31**, 1806280 (2019)
19. M. Wuttig *et al.*, Revisiting the nature of chemical bonding in chalcogenides to explain and design their properties. *Adv. Mater.* **35**, 2208485 (2023)
20. D.A. Keen, M.T.T. Dove, Local structures of amorphous and crystalline phases of silica, SiO₂, by neutron total scattering. *J. Phys.: Condens. Matter* **11**, 9263 (1999)
21. T.H. Lee, S.R. Elliott, S.R. Chemical Bonding in Chalcogenides: The Concept of Multicenter Hyperbonding. *Adv. Mater.* **32**, 2000340 (2020)]
22. J.Y. Raty, C. Otjacques, J.P. Gaspard, C. Bichara, C. Amorphous structure and electronic properties of the Ge₁Sb₂Te₄ phase change material. *Solid State Sci.* **12**, 193-198 (2010)
23. L Guarneri *et al.*, Metavalent bonding in crystalline solids: how does it collapse? *Adv. Mater.* **33**, 2102356 (2021)
24. M. Micoulaut, J.Y. Raty, C. Otjacques, C. Bichara, Understanding amorphous phase-change materials from the viewpoint of Maxwell rigidity. *Phys. Rev. B*, **81**, 174206 (2010)
25. C. Persch *et al.*, The potential of chemical bonding to design crystallization and vitrification kinetics. *Nat. Commun.* **12**, 4978 (2021)
26. A. Heßler *et al.*, In₃SbTe₂ as a Programmable Nanophotonics Material Platform for the Infrared, *Nat. Commun.* **12**, 924 (2021)
27. L. Conrads *et al.*, Reconfigurable and polarization dependent perfect absorber for large-area emissivity control based on the plasmonic phase-change material In₃SbTe₂, *Adv. Opt. Mater.* 2202696 (2023)
28. N.B.M. Schröter *et al.*, Chiral topological semimetal with multifold band crossings and long Fermi arcs. *Nat. Phys.* **15**, 759–765 (2019).
29. R.S.K Madsen *et al.*, Ultrahigh-field 67Zn NMR reveals short-range disorder in zeolitic imidazolate framework glasses. *Science* **367**, 6485 (2020)
30. A. Singh, M.K. Jana, D.B. Mitzi, Reversible crystal-glass transition in a metal halide perovskite, *Adv. Mater.* **33**, 2005868 (2021)
31. M. Wuttig *et al.*, Halide perovskites: third generation photovoltaic materials empowered by an unconventional bonding mechanism, *Adv. Funct. Mater.* **32**, 2110166 (2022)
32. W. Kohn, L.J. Sham, Self-Consistent Equations Including Exchange and Correlation Effects. *Phys. Rev.* **140**, A1133 (1965)
33. G. Kresse, J. Hafner, Ab initio molecular-dynamics simulation of the liquid-metal–amorphous-semiconductor transition in germanium. *Phys. Rev. B* **49**, 14251 (1994)
34. J.P. Perdew, K. Burke, M. Ernzerhof, Generalized gradient approximation made simple. *Phys. Rev. Lett.* **77**, 3865 (1996)
35. P.E. Blöchl, Projector augmented-wave method. *Phys. Rev. B* **50**, 17953-17978 (1994)
36. G. Kresse, D. Joubert, From ultrasoft pseudopotentials to the projector augmented-wave method. *Phys. Rev. B* **59**, 1758 (1999)

37. K. Lee, E.D. Murray, L. Kong, B.I. Lundqvist, D.C. Langreth, Higher-accuracy van der Waals density functional. *Phys. Rev. B* **82**, 081101(R) (2010).
38. S. Baroni, R. Resta, Ab initio calculation of the macroscopic dielectric constant in silicon. *Phys. Rev. B* **33**, 7017 (1986)
39. P. Giannozzi *et al.*, Advanced capabilities for materials modelling with Quantum ESPRESSO. *J. Phys. Condens. Matter.* **29**, 465901 (2017)
40. A. Otero-de-la-Roza, E.R. Johnson, V. Luaña, Critic2: A program for real-space analysis of quantum chemical interactions in solids. *Comp. Phys. Comm.* **185**, 1007-1018 (2014)
41. A. Otero-de-la-Roza, <https://github.com/aoterodelarozacritic2> (2018).
42. A.A. Mostofi *et al.*, Wannier90: A tool for obtaining maximally-localised Wannier functions. *Comput. Phys. Commun.* **178**, 685–699 (2008)
43. R. Hoppe, Effective coordination numbers (ECoN) and mean fictive ionic radii (MEFIR). *Z Kristallogr. Cryst. Mater.* **150**, 23-52 (1979)

Supporting Information for

Tailoring chemical bonds to design unconventional glasses.

Jean-Yves Raty, Christophe Bichara, Carl-Friedrich Schön, Carlo Gatti & Matthias Wuttig.

This SI Appendix file includes:

Supporting text

Figures S1 to S4

Tables S1 to S4

SI References

Supporting Information Text

1. Electron Localization and Delocalization Indexes.

In this paragraph, a concise theoretical illustration of the so-called electron localization and delocalization indexes¹, as applied to molecules and periodic and non-periodic solids, is given, followed by some details on the computations performed. The theoretical presentation is, in part, a brief summary of what has been much more extensively reported in Ref. ²

The average electron population $N(\Omega)$ of an atom Ω is given by integrating the electron density $\rho(\mathbf{r})$ over its basin, $N(\Omega) = \langle \hat{n}_\Omega \rangle = \int_\Omega \rho(\mathbf{r}) d\mathbf{r}$. In this work, we have used as atomic basins Ω those defined by the Quantum Theory of Atoms in Molecules (QTAIM) due to Bader³. Electron localization and delocalization have a statistical interpretation. They are related to the *variance* and *covariance* of the atomic populations and the corresponding localization and delocalization indices, LI and DI, are respectively given by

$$LI(\Omega) = N(\Omega) - Var(\hat{n}_\Omega) = \langle \hat{n}_\Omega \rangle - (\langle \hat{n}_\Omega^2 \rangle - \langle \hat{n}_\Omega \rangle^2) \quad (1)$$

$$DI(\Omega, \Omega') = -2Cov(n_\Omega, n_{\Omega'}) = -2(\langle \hat{n}_\Omega \hat{n}_{\Omega'} \rangle - \langle \hat{n}_\Omega \rangle \langle \hat{n}_{\Omega'} \rangle) \quad (2)$$

where $N(\Omega) \geq LI(\Omega) \geq 0$ and $DI(\Omega, \Omega') \geq 0$. For an atom Ω with electrons perfectly localized within Ω , $LI(\Omega) = N(\Omega)$ and $DI(\Omega, \Omega') = 0$ for all Ω' . The properties of variance and covariance require that $N(\Omega) = LI(\Omega) + \frac{1}{2} \sum_{\Omega' \neq \Omega} DI(\Omega, \Omega')$, for every atom Ω in the system. Hence, the average number of electrons in atom Ω can be rigorously partitioned into those that are localized, $LI(\Omega)$, and those that are *shared*.

The average values in the equations 1 and 2 are calculated by integrating the relevant one- and two-particle densities, namely the electron density $\rho(\mathbf{r})$ and the pair density $\pi(\mathbf{r}_1, \mathbf{r}_2)$. The latter may be written in terms of a product of independent electron densities and of the exchange correlation density,

$$\pi(\mathbf{r}_1, \mathbf{r}_2) = \rho(\mathbf{r}_1)\rho(\mathbf{r}_2) - \varrho_{exc}(\mathbf{r}_1, \mathbf{r}_2) \quad (3)$$

where ϱ_{exc} is a purely non-classical term measuring the deviation of the pair density from the independent-electron distribution. In a Hartree-Fock (HF) calculation the exchange-correlation density contains only the exchange contribution $\varrho_{exc}(\mathbf{r}_1, \mathbf{r}_2) = \gamma(\mathbf{r}_1, \mathbf{r}_2)\gamma(\mathbf{r}_2, \mathbf{r}_1)$ where $\gamma(\mathbf{r}_1, \mathbf{r}_2)$ is the one-electron density matrix, $\gamma(\mathbf{r}_1, \mathbf{r}_2) = \sum_i^{occ.orb} \lambda_i^2 \psi_i^*(\mathbf{r}_1)\psi_i(\mathbf{r}_2)$, and where λ_i is the occupation number of the occupied orbital ψ_i . In a Kohn-Sham (KS) DFT calculation, only $\rho(\mathbf{r})$ is available, but ϱ_{exc} is approximated by replacing ψ_i with the KS orbitals. This is a customarily done approximation

yielding DIs that are quantitatively similar to the HF ones and that are deemed to be still chemically meaningful in all those situations where strong correlation effects can be ignored ⁴ .

The LI and DI are given by the following expressions in terms of ρ_{exc}

$$LI(\Omega) = LI(\Omega, \Omega) = \int_{\Omega} \int_{\Omega} \rho_{exc}(\mathbf{r}_1, \mathbf{r}_2) d\mathbf{r}_1 d\mathbf{r}_2 \quad (4)$$

$$DI(\Omega, \Omega') = 2 \int_{\Omega} \int_{\Omega'} \rho_{exc}(\mathbf{r}_1, \mathbf{r}_2) d\mathbf{r}_1 d\mathbf{r}_2 \quad (5)$$

and it may be easily shown that for an HF calculation (hence, with approximation, also for a KS one, see above)

$$\int_{\Omega} \int_{\Omega'} \rho_{exc}(\mathbf{r}_1, \mathbf{r}_2) d\mathbf{r}_1 d\mathbf{r}_2 = \sum_{ij} S_{ji}^{\Omega} S_{ij}^{\Omega'} \quad (6)$$

where the S_{ij}^{Ω} are the matrix elements of the atomic domain Ω overlap matrix,

$$S_{ij}^{\Omega} = \int_{\Omega} \lambda_i \lambda_j \psi_i^*(\mathbf{r}_1) \psi_j(\mathbf{r}_1) d\mathbf{r}_1 \quad (7).$$

Thus, the S_{ij}^{Ω} are the key ingredients to evaluate both LIs and DIs. While the atomic domain overlap matrices are complex Hermitian matrices whose elements depend on the particular set of orbitals that have been adopted to describe a system, Eq. 6 gives rise to the elements $\Omega\Omega'$ of a real symmetric matrix that is invariant to orbital rotations and so are as a consequence both the LI and the DIs.

Evaluation of Eq 4 and 5 is easily affordable for molecular systems, but becomes instead extremely cumbersome in the solid state, because the number of atomic domain overlap matrices in infinite periodic solids makes their calculation much more challenging and heavier.

Baranov and Kohout⁵ and later Golub and Baranov⁶ have proposed a viable, yet computationally demanding approach, to evaluate LIs and DIs in condensed systems in the context of augmented-plane-wave and of projector-augmented-wave (PAW) wave functions, respectively. Both these approaches use Bloch orbitals or states $\psi_{nk}(\mathbf{r})$ in the calculation of the atomic domain overlap matrices

$$\psi_{nk}(\mathbf{r}) = u_{nk}(\mathbf{r}) e^{ik \cdot \mathbf{r}} \quad (8)$$

written as a truncated expansion in augmented plane-waves. In Eq. 8 \mathbf{k} is a vector in the first Brillouin zone, n is the band index and the Bloch states are separated into a periodic part $u_{nk}(\mathbf{r})$ and a phase $e^{i\mathbf{k}\cdot\mathbf{r}}$ thanks to Bloch's theorem. In the present work we have adopted, instead, a more recent and much faster approach due to Otero-de-la-Roza, Martín Pendás and Johnson² that adopts Maximally Localized Wannier Functions^{7,8} to bypass the calculation of all atomic overlaps related to functions whose centers are sufficiently far apart. Wannier functions⁹ are real-space alternatives of Bloch states and are obtained from these latter through the transformation

$$w_{n\mathbf{R}}(\mathbf{r}) = \frac{V}{(2\pi)^3} \int \psi_{nk}(\mathbf{r}) e^{-i\mathbf{k}\cdot\mathbf{R}} d\mathbf{k} \quad (9)$$

where the integration is over the first Brillouin zone and \mathbf{R} is a real space vector. Wannier functions constitute a representation of a periodic system's electronic wave function that is completely equivalent to the one obtained using extended Bloch states. MLWFs are the result of a peculiar Wannier transformation (Eq. 9) where the Bloch states are rotated

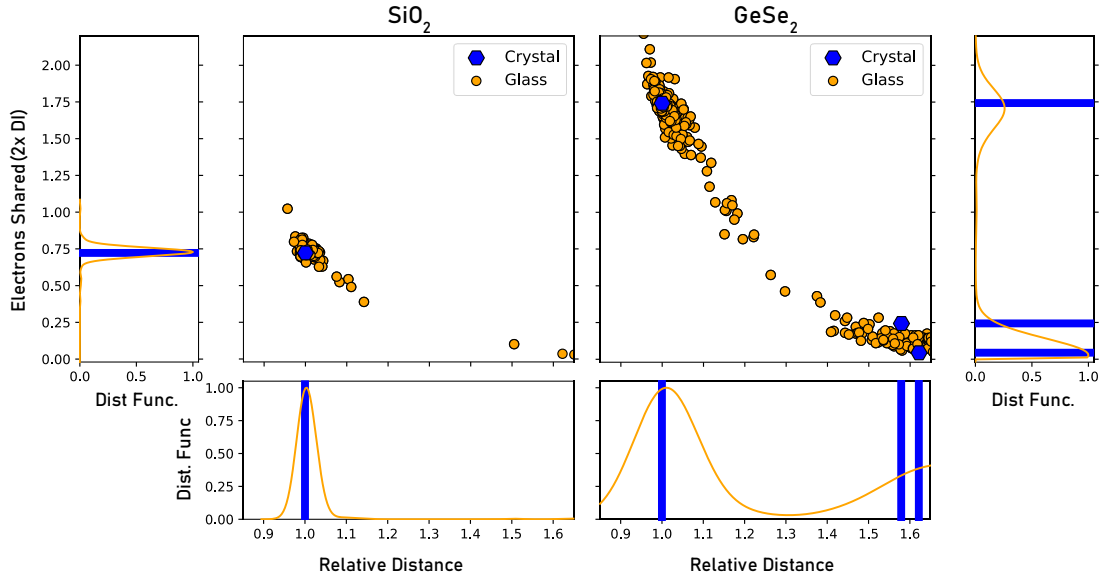
$$\tilde{\psi}_{nk}(\mathbf{r}) = \sum_m \mathbf{U}_{nm}^k \psi_{mk}(\mathbf{r}) = e^{i\mathbf{k}\cdot\mathbf{r}} \sum_m \mathbf{U}_{nm}^k u_{mk}(\mathbf{r}) \quad (10)$$

so that the combined spread of all the resulting Wannier functions is minimized⁷. MLWFs are the solid-state analogue of the Foster and Boys localized molecular orbitals¹⁰. Atomic domain overlap matrices in terms of Wannier functions (either standard or MLWFs) are given by

$$S_{n\mathbf{R},n'\mathbf{R}'}^{\Omega+\mathbf{R}''} = \int_{\Omega+\mathbf{R}''} w_{n\mathbf{R}}^*(\mathbf{r}) w_{n'\mathbf{R}'}(\mathbf{r}) d\mathbf{r} \quad (11)$$

where $\Omega + \mathbf{R}''$ is an atom Ω translated by lattice vector \mathbf{R}'' , n and n' are band indices, and $\mathbf{R}, \mathbf{R}', \mathbf{R}''$ are lattice vectors. From a comparison of Eq. 11 and Eq. 7 it is clear that the number of atomic overlaps to be calculated for a periodic solid becomes much higher than in the molecular case. As a clarifying example, a few billions of atomic overlaps are required to calculate all of the DIs in the urea crystal, while only a few thousands of them are needed for the *in vacuo* urea molecule. To be able to calculate the DIs even for the simplest solids, one has to avoid the calculation of as many atomic overlaps as possible and to compute the non-negligible overlap integrals very efficiently. Using MLWFs a significant number of atomic overlap integrals can be discarded *a priori* and equated to zero as the integral in eq. 11 is assumed to give a negligible contribution if the distance between the MLWFs centers is high enough (for technical/computational details see Ref. ²).

2. DI vs distance in glasses



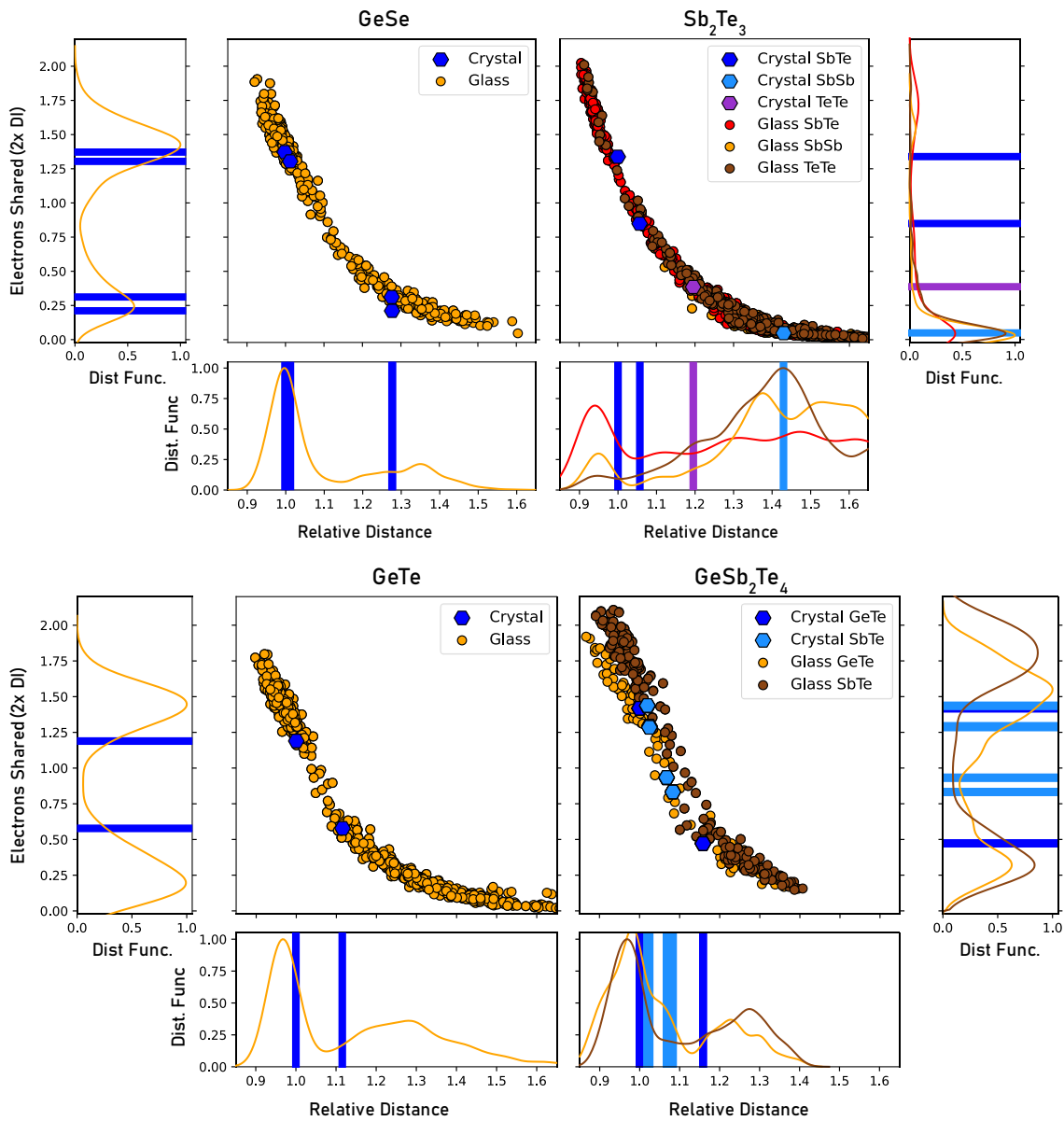


Fig. S1. For each system, the square panel shows the delocalization index (DI) values as a function of inter-atomic distance (rescaled to the shortest corresponding distance in the crystal.). The vertical and horizontal panels show the distribution of DI and of distances, respectively, the values for the crystal being indicated by the bars. The difference between distributions in the crystal and in the amorphous appear clearly for GeTe and GeSb₂Te₄ (GST). In the case of GeSe, both distance and DI distributions have peaks located very close to those of the crystal, as it is observed for GeSe₂. Upon ageing, the DI distribution of glassy GeTe evolves and becomes even more distinct from the crystal as illustrated in Figure S2.

3. Relation between aging and localization in GeTe

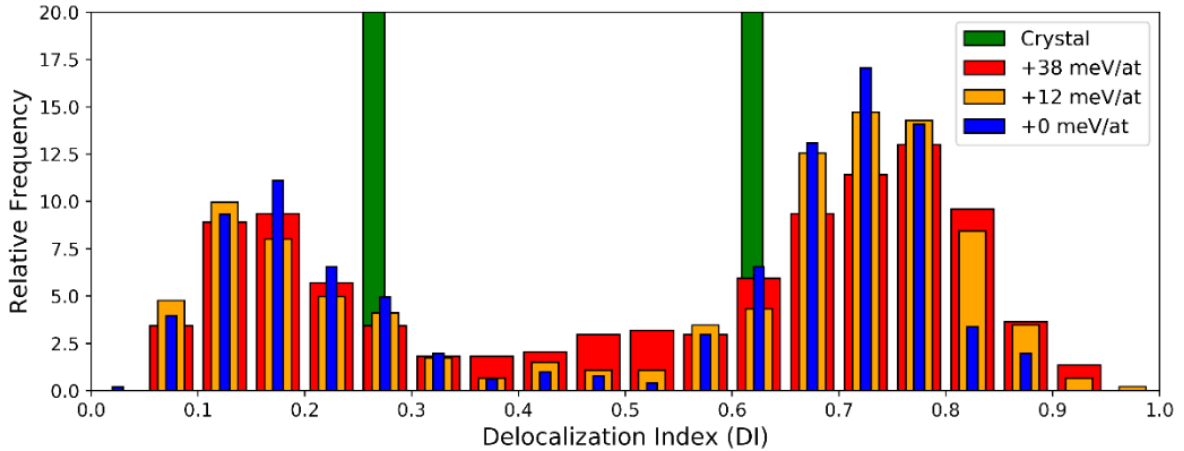


Fig. S2. Detailed distributions (vertical panels in Fig 1B) for various GeTe amorphous models. Upon ageing, the total energy (given in the legend) of the structure decreases¹¹, the evolution of the distribution is characterized by better defined peaks in the lowest energy structure (around DI=0.18 and DI=0.73) with a clear decrease in bonds with DI 0.35-0.55 (0.7 to 1.1 electron share). This subtle variation is not linked with the small proportion of homopolar bonds. See Ref. ¹¹ for a detailed description of the structural evolution.

4. Extended discussion of the relationship between structure and bonding

In the main manuscript, Figure 1 displays the number of electrons shared ES, which is twice delocalization index (DI) value, against internuclear Ge-Te distances for the most stable GeTe amorphous structure. A large number of different DI values is obtained for the different atomic distances found in the glass. For the sake of comparison, data at the two Ge-Te distances found in the crystalline GeTe structure (at 0 K) are also indicated. As expected the electron sharing is decreasing with increasing atomic separation and decreasing covalent character of the bonding. This figure quantifies the common belief that the bond length scales with the bond strength. A similar behavior was recently reported by Lee and Elliott¹² for a number of chemical-bonding indicator data, calculated at the Ge-Te and Sb-Te homopolar bond critical points (BCPs) in simulated models of amorphous and crystalline GST. Common to the present study and the one by Lee and Elliott it is the fact that the property data for the crystal structures exactly fall on the property evolution curves obtained from the wider range and (much) more numerous datapoints of the related amorphous structures. This observation brought Lee and Elliot to conclude that the “surprising similarity (of properties) indicates that interatomic interactions in c-GST are indistinguishable from (some of) those in a-GST; more precisely, chemical-bonding interactions in c-GST belong to a subgroup of the broad spectrum of interactions existing in a-GST, but are not a different type of interaction to those present in a-GST”. We are indeed not surprised by the similarity of properties of bonding in amorphous and crystalline structures when they are evaluated *at a common geometry*. This is purely a consequence of the local character of the properties being

examined. Those properties considered by Lee and Elliot are local in nature since they refer to a precise point, the BCP, taken as the most representative point along the bond path joining the two bonded nuclei³. The DIs, despite being the result of an integration of the exchange correlation density over the two atomic basins of the bonded atoms, are known to be also fundamentally local in character because of the short-range nature of electron delocalization¹³.

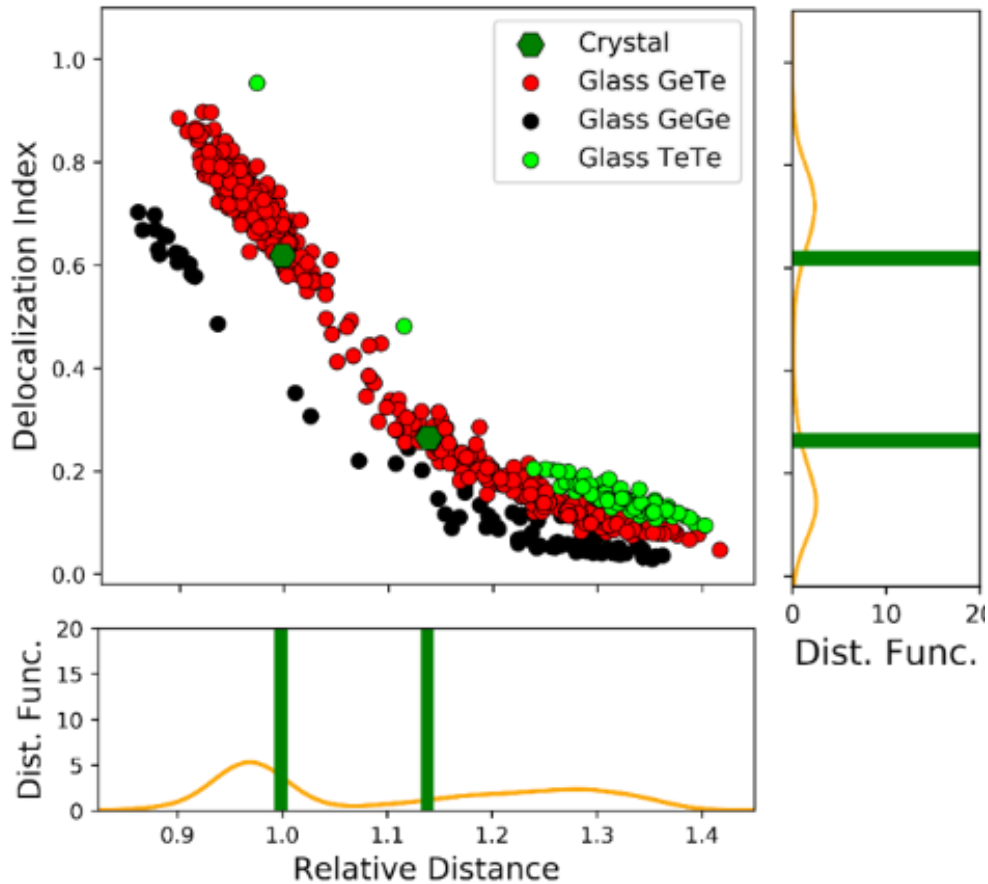


Fig. S3. Delocalization Index (DI) values (first six neighbors) for low energy amorphous GeTe. Ge-Te, Ge-Ge and Te-Te bonds are plotted in red, black and green, respectively. The distributions of the DIs and of the distances values are plotted on the right and below the main panel. The green bars indicate the crystal values. One can notice the large deviation between average DI in the amorphous and in the crystal, linked with smaller interatomic distances.

It is hence no surprise that the same (local) atomic arrangement in the glass and the crystal is accompanied by the same chemical bonding descriptors. This is the essence of the Zachariasen conjecture, the similarity of chemical bonding in the glass and the crystal leads to a similarity in atomic arrangement. Yet, for glasses like GeTe and GeSb₂Te₄, it has been long known that the atomic arrangement differs considerably from the corresponding crystal. This can only be explained if there are significant differences in bonding between the glass and the crystal. Figure 1 shows convincingly that this is indeed the case.

It is the peak(s) height, position and width of interatomic distance distributions that drastically distinguishes amorphous and crystal structures, thus leading to their quite distinct “average” bonding features and properties. In particular, differently from the amorphous case, the peaks of crystal GeTe have zero width and positions that almost correspond to the larger and lower internuclear distances found for the low and large internuclear distance groups in the amorphous structure. As a consequence, the two distinct peaks, having the same height but quite different DI values (0.25 and 0.65) in the crystal (Fig. S2 and S3), are replaced by two very broad and shallow peaks in the amorphous structure. Each of them has DI values distributed in a range that is roughly as large as it is the DI difference between the two distinct peaks in the crystal.

5. Measuring the deviation from the Zachariasen character

To define an order parameter NZ characterizing the difference between crystal and amorphous local environments, we use the distributions of the first distances around each kind of atom obtained from Molecular Dynamics simulations. These distributions overlap (Figure 2a, Figure S4a-f) and their averages (Figure 2b, c) and fluctuations are used to calculate NZ in the following way. For each atom of species j in the structure, we identify its N_j first neighbors, and create N_j histograms of these distances, once they are sorted. NZ is defined as a sum of partial contributions Z_j from the N_{sp} atomic species:

$$NZ = \sum_{j=1}^{N_{sp}} c_j Z_j$$

$$Z_j = S \left\langle \frac{1}{N_j} \sum_{i=1}^{N_j} \left(\frac{d_i^A - d_i^C}{d_i^C} \right)^2 \right\rangle^{1/2}$$

c_j is the concentration of species j , S is a scaling factor to set NZ between 0 and 1 ($S = 25$ here). We choose $N_j = 6$ for all systems, although SiO_2 and GeSe_2 are tetrahedrally bonded crystals whereas GeSe , GeTe , GeSb_2Te_4 are octahedrally bonded (rhombohedral and orthorhombic structures). In any case, the inclusion of the 5th and 6th neighbor contribution in SiO_2 and GeSe_2 is slightly increasing the value of NZ (see Table S6.2). The terms in the sum are the squared relative difference of the averaged i^{th} bond lengths (d_i^C , d_i^A) between crystal and amorphous. The values of the parameters obtained from Molecular Dynamics and resulting Z_j and the contributions to NZ are given in Supplementary Tables S2 and S3.

6. Neighbors distributions in glasses vs crystals.

Here we present the distance analysis for all 6 systems and all species. In each case, we plot on the top panel the distributions of the first six normalized distances around a given species in both the glassy (orange) and crystalline (green) phases. From these, the average distances shown in the corresponding bottom panel have been computed.

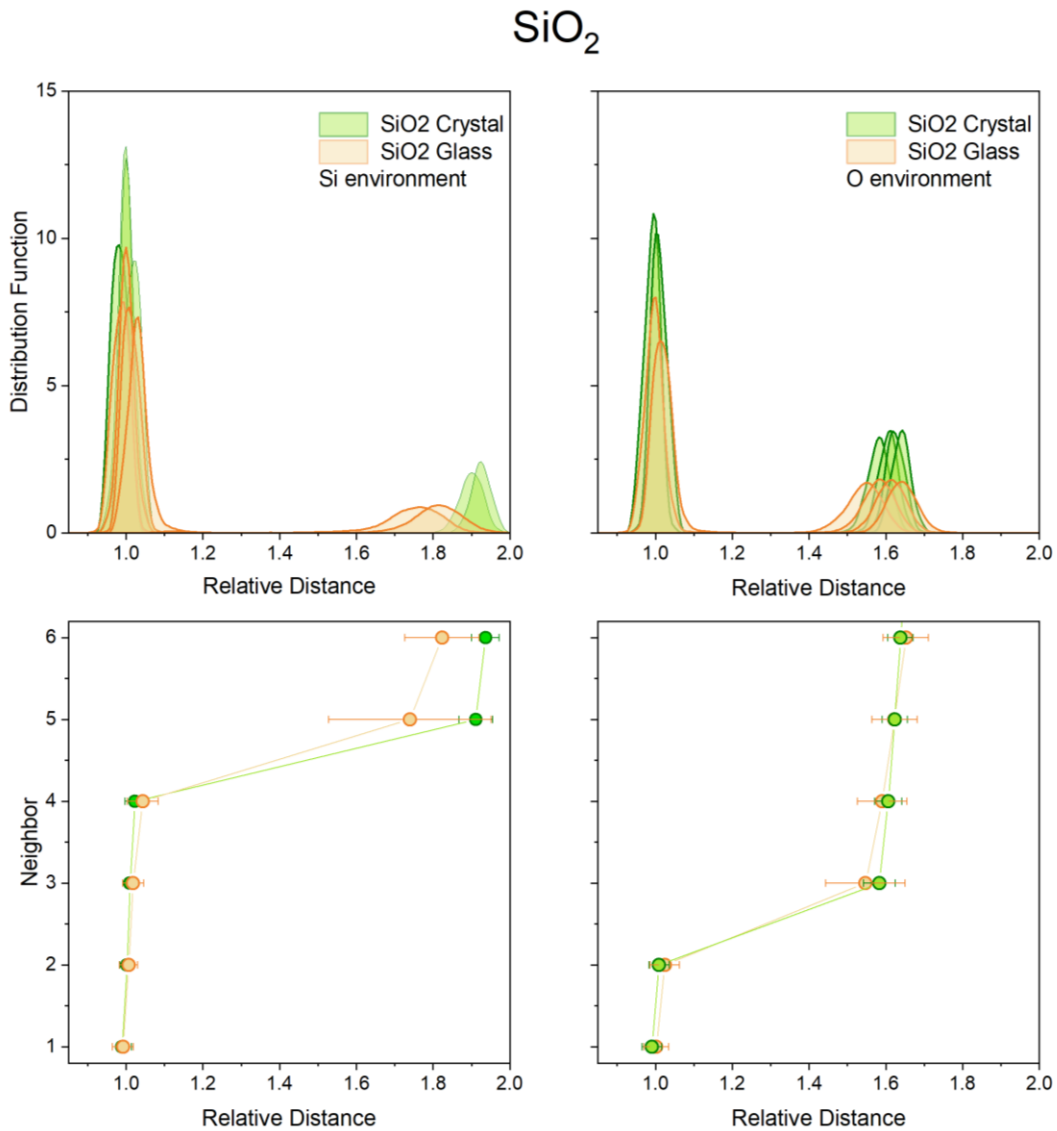


Fig. S4.a. The SiO_2 glass is almost perfectly tetrahedrally coordinated. Only angular fluctuations are responsible for the broader/shorter 5th and 6th distance distributions.

GeSe₂

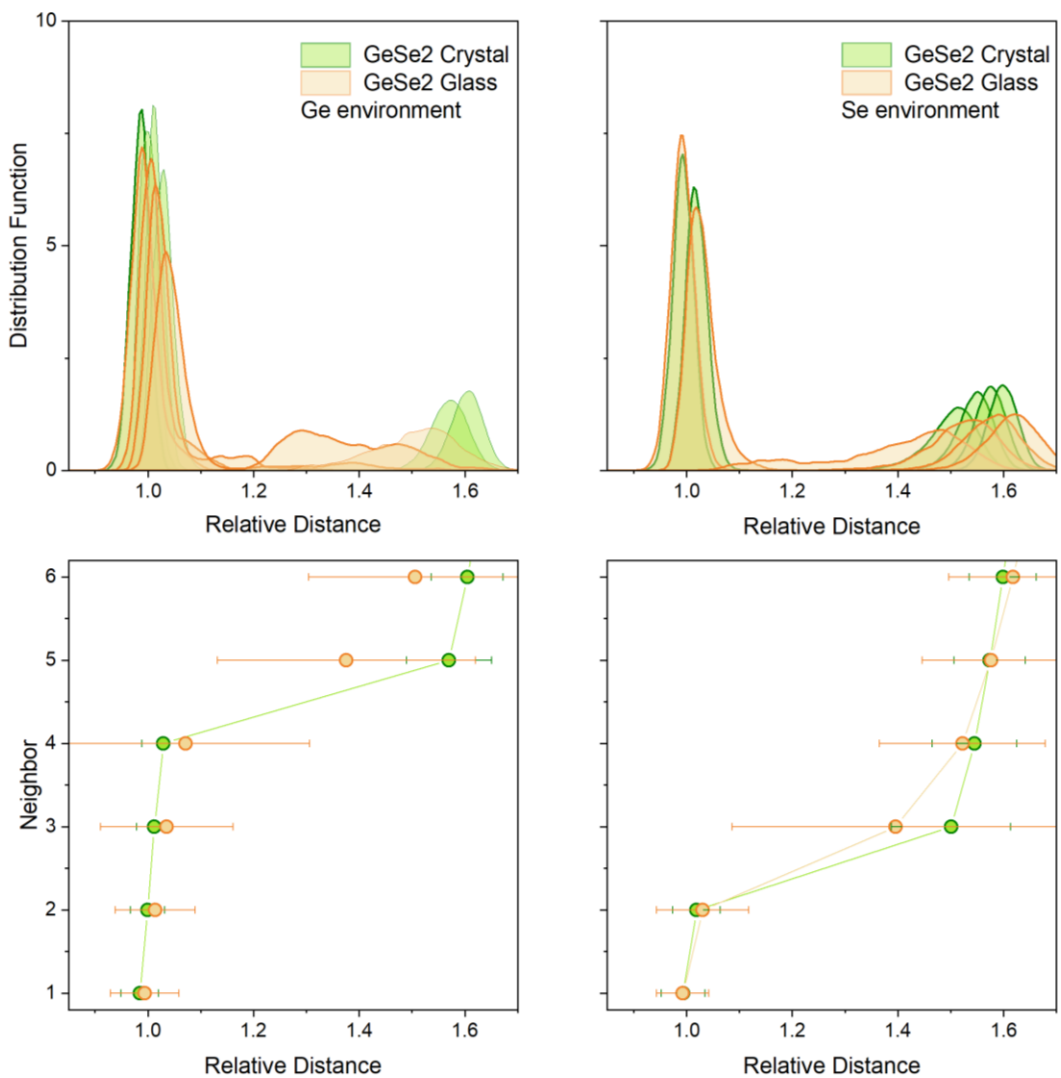


Fig. S4.b. In glassy GeSe₂, the tetrahedral nature of the local order around Ge atoms is preserved, as well as the two-fold coordination of the Se atoms. Coordination defects (linked to the presence of a few homopolar bonds) are responsible for the larger distribution of the 4th and 5th neighbor of Ge atoms, and the 3rd neighbor distribution for O atoms.

GeSe

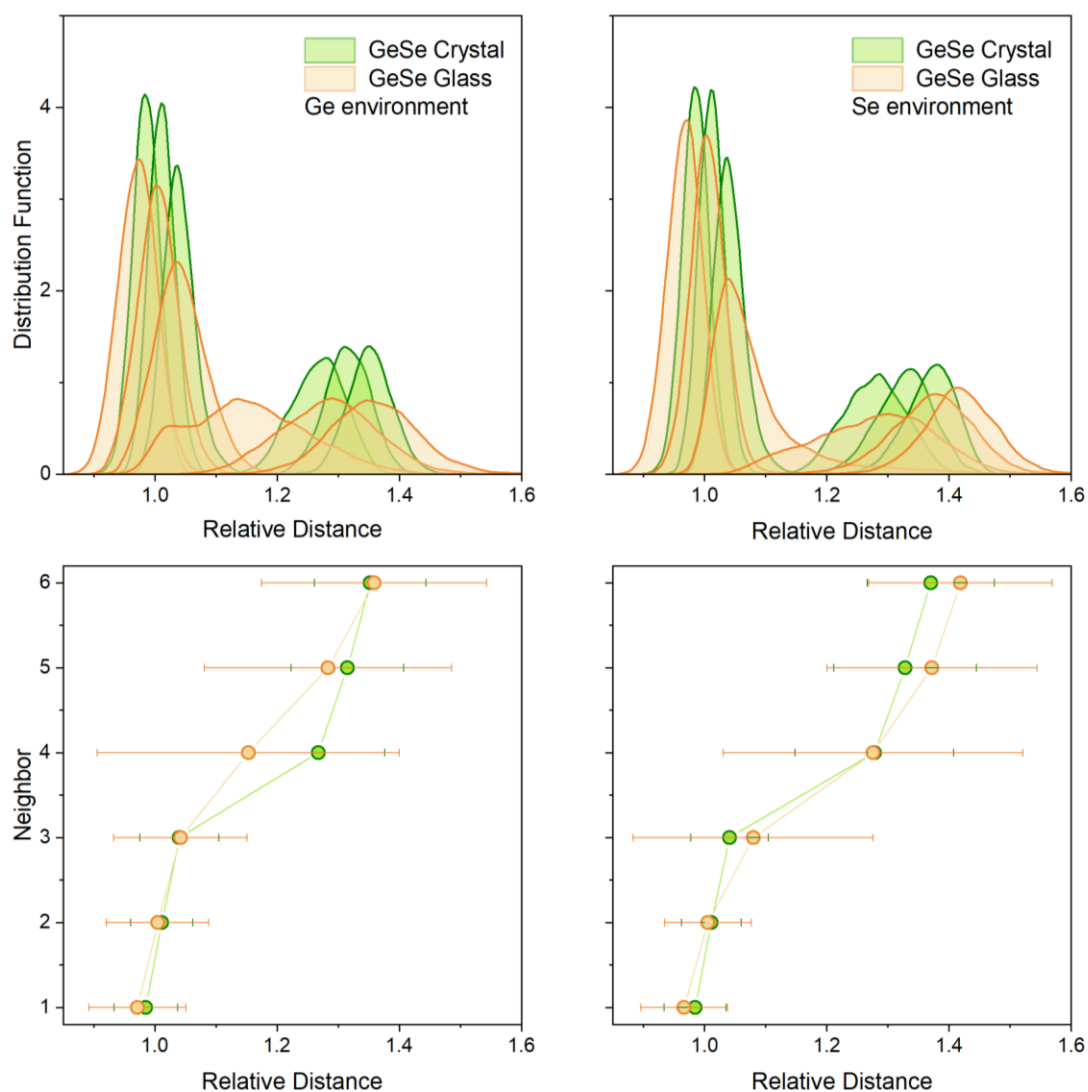


Fig. S4.c. The GeSe crystal is orthorhombic and the structure derives from a Peierls distortion of a cubic structure. As a consequence, shorter and longer bonds are found and the local Ge and Sb environment is a '2+1 / 1+2' distorted octahedron. In the glass, the local order appears quite similar, with a '3+3' effective coordination of both Ge and Sb atoms. The presence of a few homopolar Ge-Ge bonds causes the broader distribution of the 4th Ge neighbor (bimodal distribution).

GeTe

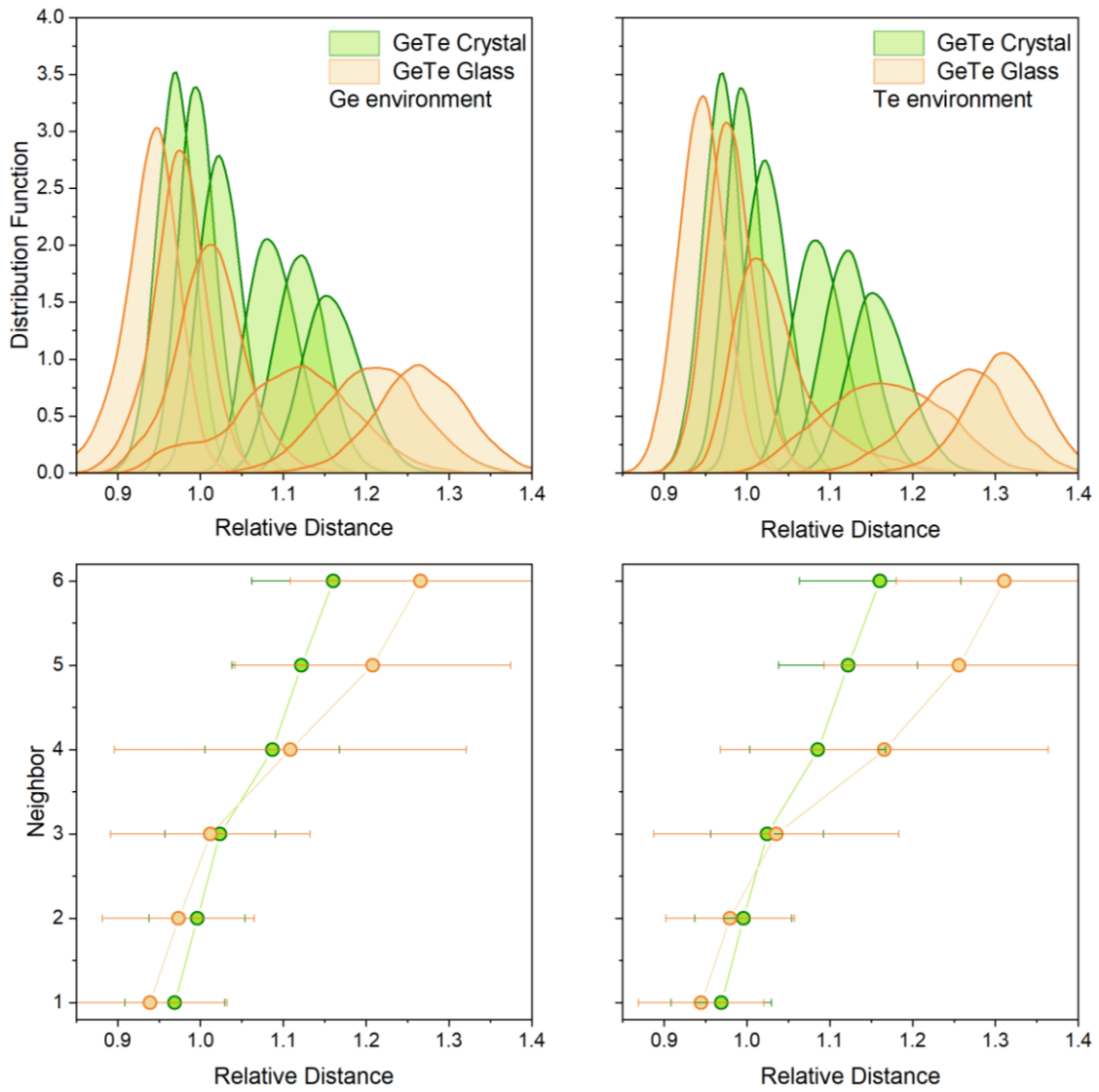


Fig. S4.d. The R-3m crystalline structure of GeTe corresponds to a '3+3' coordination in a distorted octahedral geometry. In the amorphous (as described in Ref. ¹¹, for instance), the dominant order remains octahedral, but with much larger Peierls distortion ratio (the short distances are shorter, and the long ones are longer in the amorphous phase). Furthermore, the coordination number is smaller (tends toward 3 for both Ge and Te atoms). Here, the broader 4th neighbor distribution around Ge atoms is due to a bimodal distribution (few tetrahedral Ge atoms, with Ge-Ge homopolar bonds).

Sb_2Te_3

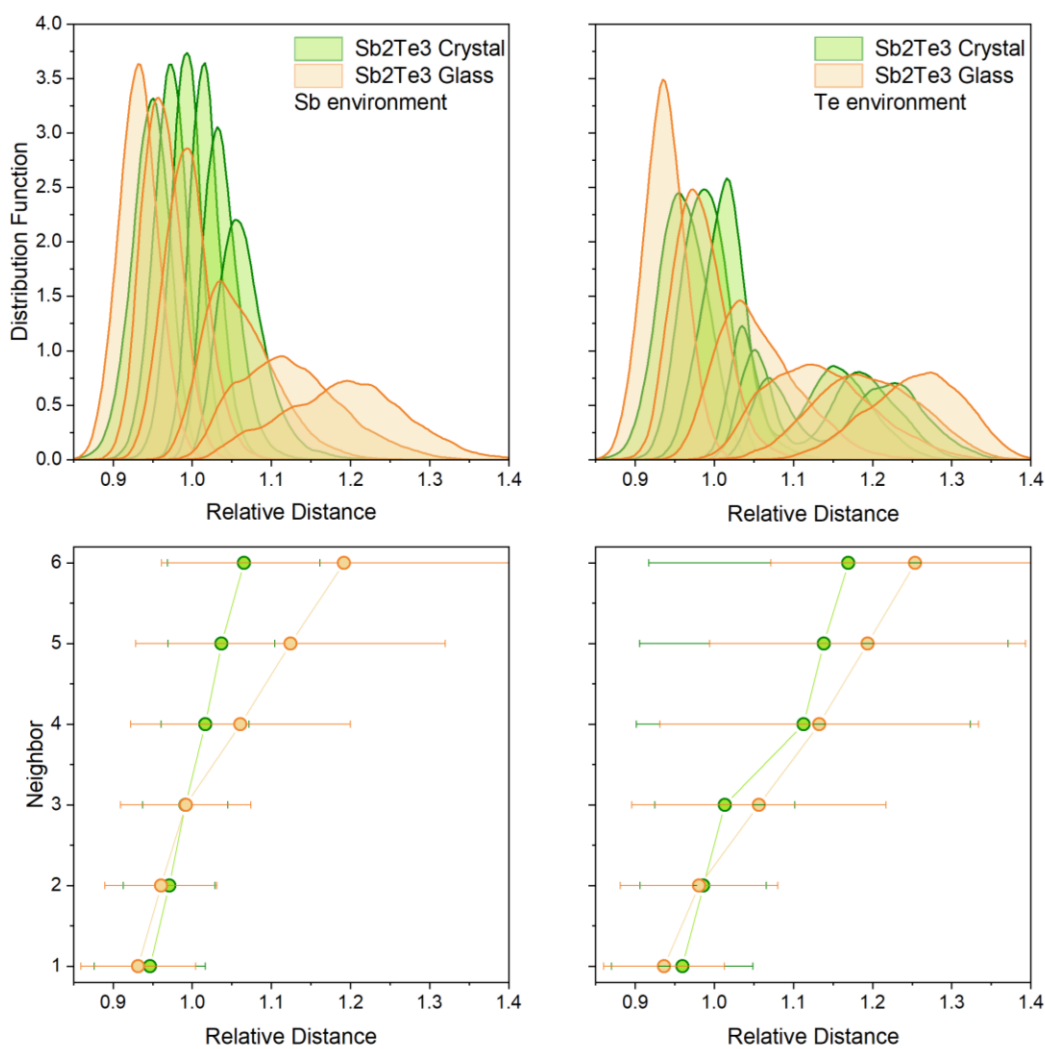


Fig. S4.e. In the R-3m crystalline structure of Sb_2Te_3 , each atom is locally octahedrally bonded. Around Sb atoms, 6 equal bonds are found, whereas two types of Te sites exist. 1/3 of the Te atoms have '3+3' Sb neighbors, the remaining 2/3 of Te having 3 short Sb-Te bonds and 3 longer Te-Te bonds. The structure of the glass is very different. For the Sb atoms, the coordination is much lower with 3 short Sb-Te bonds. Te atoms also have a lowered average coordination.

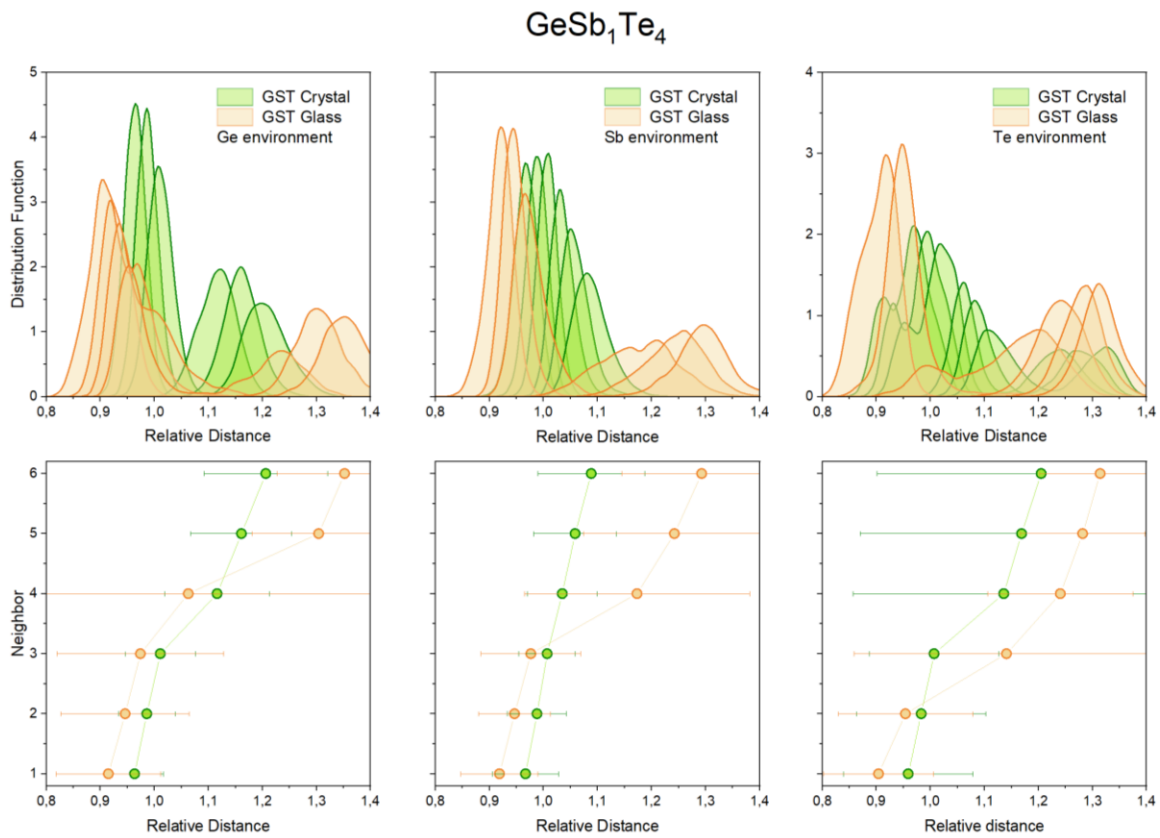


Fig. S4.f. The R-3m crystalline structure of GeSb₂Te₄ is layered with local octahedral order. Due to Peierls distortions, Ge atoms have a '3+3' coordination, Sb have 6 first neighbors and two Te sites exist as for Sb₂Te₃.

In the glass, Ge atoms have 3 or 4 first neighbors (broad 4th neighbor, and a bimodal distribution due to the presence of a few homopolar bonds). Sb atoms are 3-fold coordinated and Te atoms are either 2- or 3-fold coordinated.

Table S1. Structural data for glasses and crystals at finite T.

Interatomic distance (maximum of the partial $g(r)$), coordination number (cutoff from minimum of partial $g(r)$ in column 1), representative angle (width from a gaussian fit). All amorphous and crystal values are obtained from averaging over trajectories at 300K.

	R1 (Å)	R1 (Å, litt.)	Coordination number (cutoff Å)	Z (Litt)	Angle (σ)
SiO₂ Glass	SiO: 1.63 SiSi: 2.99 OO: 2.63	[¹⁴] SiO:1.62 SiSi:3.1	Si : Z=4.01 (2.0Å) O : Z=2.01	[¹⁴] Si: Z=4 O: Z=2 O-Si-O 109°	O-Si-O 109° (13) 100% Corner Sharing
SiO₂ Crystal 300K	SiO: 1.62 SiSi: 3.14 OO: 2.64		Si : Z=4 (2.0Å) O : Z=2		O-Si-O: 109° (7) 100% Corner Sharing
GeSe₂ Glass	GeSe: 2.42 GeGe: 2.52 SeSe: 2.36	[^{15,16}] 2.37, 2.36 2.45, 2.42 2.36, 2.32	Ge : Z=3.89 (3.14Å) 0.23Ge+3.65Se Se : Z=2.10 1.83Ge+0.27Se Ge : 89% Z=4 10% Z=3 Se : 89% Z=2 10% Z=3	[¹⁶] Ge : Z=3.96 0.25Ge+3.71Se Se : Z=2.05 1.86Ge+0.20Se	Ge-Se-Ge : 80° (12)+100°(8) Se-Ge-Se : 109° (21)
GeSe₂ Crystal 300K (Ortho.)	GeSe: 2.41		Ge : Z=4 (2.95Å) Se : Z=2		Ge-Se-Ge 100° (8) Se-Ge-Se 109° (17)
GeSe Glass	GeSe: 2.57 GeGe: 3.67 SeSe: 3.81		Ge : Z=3.41 (3.0Å) 0.53Ge+2.89Se 58% Z=3 38% Z=4 2% Z=2 Se: Z=2.89 2.89 Ge 74% Z=3 19% Z=2 7% Z=4		Ge-Se-Ge : 89° (29) Se-Ge-Se : 95.0° (18)
GeSe Crystal 300K	GeSe: 2.61 GeGe: 3.60 SeSe : 3.80		Ge : Z=3 (3.0Å) Se : Z=3		Ge-Se-Ge : 101° (11) Se-Ge-Se : 94° (8)
Sb₂Te₃ Glass	SbTe: 2.97 TeTe : 4.18	[¹⁷] SbTe:2.9 4 TeTe: 4.25	Sb: Z=4.87 (3.56Å) 0.78Sb+4.09Te 28% Z=4 44% Z=5 23% Z=6	[¹⁷] Sb: Z=5.2 (3.9Å) 0.6Sb+4.6Te	Sb-Te-Sb 85° (9) Te-Sb-Te 91° (12)

	R1 (Å)	R1 (Å, litt.)	Coordination number (<i>cutoff</i> Å)	Z (Litt)	Angle (σ)
			Te : Z=3.90 2.73Sb+1.17Te 6% Z=2 30% Z=3 37% Z=4 21% Z=5, 6% Z=6	Te Z=3.5 3.1Sb+0.7Te ~90° angles.	
Sb₂Te₃ Crystal 300K	SbTe: 3.06 TeTe: 3.53		Sb : Z=6.0 (3.56Å) Te : Z=5.15 4.0Sb +1.15Te 19% Z=4 24% Z=5 49% Z=6		Sb-Te-Sb 93° (9) Te-Sb-Te 91° (8)
GeTe Glass	GeTe: 2.78 GeGe:2.6 1 TeTe: 4.02		Ge: Z=3.29 (3.12Å) 0.35Ge+2.94Te 63% Z=3 31% Z=4 4% Z=2 Te: Z=2.96 0.02Ge+2.94Te 72% Z=3 12% Z=4 16% Z=2		Ge-Te-Ge 89° Te-Ge-Te 93° (16)
GeTe Crystal 300K	GeTe: 2.87+3.20		Ge: Z=6 (3+3) (3.66Å) Te : Z=3 (3+3)		Te-Ge-Te 94° (8) Ge-Te-Ge 93° (9)
GeSb₂Te₄ Glass	GeTe: 2.68 SbTe:2.85 TeTe:4.07	[¹⁸] GeTe: 2.61 SbTe: 2.83	Ge:Z=3.48 (3.26Å) 0.4Ge+0.3Sb+2.78Te 46% Z=3 51% Z=4 3% Z=2 Sb:3.06 0.2Ge+0.3Sb+2.61Te 92% Z=3 7% Z=4 Te: Z=2.15 0.7Ge+1.31Sb+0.16Te	[¹⁹] Ge: Z=3.9 Sb: Z=2.8 Te: Z=2.4 [¹⁸] Ge: Z=3.91 Sb: Z=2.91 Te: Z=1.98	Ge-Te-Ge 89°+100° Te-Ge-Te 101°(22) Sb-Te-Sb 95°(17) Te-Sb-Te 96°(18)
GeSb₂Te₄ Crystal 300K	GeTe: 2.80 SbTe: 3.02 TeTe: 4.33		Ge: Z=3.05 (3.05Å) Sb: Z=6 (3.63Å) Te: Z=3.84 (3.63Å)		Ge-Te-Ge 99.4° (8) Te-Ge-Te 99.4°(8) Sb-Te-Sb 90.6°(13) Te-Sb-Te 90.5°(9)

Table S2. Partial and total Non Zachariasen parameters for all systems studied

As the NZ parameter is a measure of the difference between amorphous and crystalline local orders, a clear splitting is observed between covalent systems with $NZ \leq 0.4$ and incipient metals with $NZ \geq 0.55$. Averages for GeTe and GST are 0.764 and 0.868, respectively. Among the various structures, that sample labelled GeTe2 has the lowest total energy, corresponding to the smallest proportion of homopolar bonds and tetrahedral defective Ge atoms. This shows that independent of homopolar defective bonds, the GeTe glass has a much larger NZ value than 'regular' Zachariasen glasses. $Z1, Z2, Z3$ indicate the various species, and Z_{Av} is the value averaged over the various models.

These data are used to produce fig.2, panel d.

System	N_j	Z1	Z2	Z3	Z	Z_{Av}
SiO₂	6	0.451	0.143		0.245	
GeSe₂	6	0.207	0.302		0.271	
GeSe	6	0.394	0.267		0.330	
Sb₂Te₃	6	0.589	0.564		0.574	
GeTe1	6	0.609	0.924		0.767	0.764
GeTe2	6	0.527	0.805		0.666	
GeTe3	6	0.617	0.982		0.800	
GeTe4	6	0.720	0.925		0.823	
GST124a	6	0.831	1.173	0.805	0.914	0.868
GST124b	6	0.592	1.106	0.737	0.822	

Table S3: Partial contributions to Z_j in covalent systems.

$$D_i = \left(\frac{d_i^A - d_i^C}{d_i^C} \right)^2, \text{ with } i \text{ indicating the neighbor (sorted by increasing distance).}$$

System		D1	D2	D3	D4	D5	D6
SiO₂	Si	1.4E-5	1.8E-5	7.4E-5	1.2E-4	8.1E-3	3.4E-3
	O	3.0E-5	8.0E-5	7.6E-4	2.6E-4	4.6E-5	2.2E-6
GeSe₂	Ge	8.7E-5	2.0E-4	5.3E-4	1.7E-3	1.5E-2	3.8E-3
	Se	7.0E-7	1.3E-4	4.9E-3	2.2E-4	2.6E-6	1.4E-4
GeSe	Ge	1.9E-4	4.3E-5	3.8E-6	8.1E-3	5.8E-4	2.2E-5
	Se	3.3E-4	3.1E-5	1.4E-3	2.3E-6	1.1E-3	1.2E-3
Sb₂Te₃	Sb	7.4E-4	4.2E-4	6.1E-5	1.2E-3	5.5E-3	1.2E-2
	Te	1.1E-3	2.0E-4	1.2E-3	1.8E-3	4.4E-3	9.5E-3
GeTe1	Ge	2.2E-3	2.1E-3	2.2E-3	5.6E-4	6.4E-3	8.0E-3
	Te	1.3E-3	1.2E-3	1.8E-5	1.1E-2	1.9E-2	1.7E-2
GeTe2	Ge	9.2E-4	5.2E-4	1.3E-4	4.3E-4	5.9E-3	8.1E-3
	Te	6.5E-4	2.6E-4	1.3E-4	5.5E-3	1.4E-2	1.6E-2
GeTe3	Ge	3.4E-3	2.5E-3	2.0E-3	1.4E-3	5.1E-3	7.6E-3
	Te	1.8E-3	8.2E-4	1.1E-3	1.3E-2	1.9E-2	1.9E-2
GeTe4	Ge	5.8E-3	4.0E-3	3.2E-3	2.1E-3	5.8E-3	8.9E-3
	Te	2.6E-3	1.2E-3	1.3E-3	1.2E-2	1.7E-2	1.5E-2
GST124a	Ge	3.0E-3	2.2E-3	2.3E-3	2.2E-3	1.6E-2	1.4E-2
	Sb	2.5E-3	2.1E-3	1.3E-3	1.5E-2	2.7E-2	3.1E-2
	Te	3.3E-3	1.2E-3	1.5E-2	1.1E-2	1.1E-2	9.3E-3
GST124b	Ge	1.3E-3	9.7E-4	6.0E-4	3.3E-4	7.9E-3	9.2E-3
	Sb	2.2E-3	1.9E-3	9.9E-4	1.2E-2	2.4E-2	2.9E-2
	Te	2.9E-3	1.3E-3	1.1E-2	8.2E-3	1.0E-2	8.7E-3

Table S4. Properties tables

These data are used to produce fig.3. Z^* is the Born effective charge of the cation (averaged for the amorphous phase) obtained as one third of the trace of the Z^* tensor, given for Sb atoms in GST). E_{max} and H_{max} are the position (in energy) and height of the first peak of the imaginary dielectric function. ν_{max} is the maximal vibration frequency. The effective coordination number E_{CoN} is given for the cation (Sb in Sb containing cases). (*) In the DFT calculations, crystalline Sb_2Te_3 being metallic and glassy Sb_2Te_3 having close to 0 eV gap, such that dielectric properties have not been obtained. Hence, for Sb_2Te_3 the experimental data from Ref.²⁰ were used.

	ϵ_{∞}	Z^* (e)	$E(\epsilon_2^{\text{Max}})$ (eV)	ϵ_2^{Max}	$\nu_{\text{max}}(\text{THz})$	ECoN
SiO₂ glass	2.54	3.28	10.12	2.58	40.33	3.98
SiO₂ crystal	2.22	3.59	9.67	2.89	32.94	4
<hr/>						
GeSe₂ glass	6.20	2.20	5.03	7.40	9.53	3.82
GeSe₂ crystal	5.57	2.51	4.03	10.56	9.46	4
<hr/>						
GeSe glass	12.10	2.26	3.36	13.87	8.54	3.54
GeSe crystal	14.22	3.10	2.94	21.52	6.68	3.09
<hr/>						
Sb₂Te₃ glass	21*	4*	1.64	26.18	5.45	4.32
Sb₂Te₃ crystal	41*	11*	1.31	90.15	4.83	5.84
<hr/>						
Ge₁Sb₂Te₄ glass	24.30	2.43	1.85	20.75	7.50	3.54
Ge₁Sb₂Te₄ crystal	52.36	6.80	1.59	73.19	5.78	4.64
<hr/>						
GeTe glass	23.07	2.24	2.27	23.75	8.60	3.53
GeTe crystal	75.91	5.26	1.36	93.12	3.94	5.18

SI References

1. X. Fradera, M.A. Austen, R.W.F. Bader, The Lewis model and beyond. *J. Phys. Chem. A* **103**, 304-314 (1999)
2. A. Otero-de-la-Roza, A.P. Pendás, E.R. Johnson, Quantitative electron delocalization in solids from maximally localized Wannier functions. *J. Chem. Theory Comput.* **14**, 4699-4710 (2018)
3. R. F. W. Bader, *Atoms in molecules: A quantum theory* (Clarendon Press, Oxford, 1990)
4. X. Fradera, J. Poater, S. Simon, M. Duran, M. Solà, Electron-pairing analysis from localization and delocalization indices in the framework of the atoms-in-molecules theory. *Theor. Chem. Acc.* **108**, 214-224 (2002)
5. A.I. Baranov, M. Kohout, Electron localization and delocalization indices for solids. *J. Comput. Chem.* **32**, 2064–2076 (2011)
6. P. Golub, A.I. Baranov, Domain overlap matrices from plane-wave-based methods of electronic structure calculation. *J. Chem Phys.* **145**, 154107 (2016)
7. N. Marzari, D. Vanderbilt, Maximally localized generalized Wannier functions for composite energy bands. *Phys. Rev. B*, **56**, 12847 (1997)
8. N. Marzari, A.A. Mostofi, J.R. Yates, I. Souza, D. Vanderbilt, Maximally localized Wannier functions: Theory and applications. *Rev. Mod. Phys.* **84**, 1419 (2012)
9. G.H. Wannier, The structure of electronic excitation levels in insulating crystals. *Phys. Rev.* **52**, 191 (1937)
10. J.M. Foster, S. Boys, Canonical configurational interaction procedure. *Rev. Mod. Phys.* **32**, 300 (1960)
11. J.Y. Raty *et al.*, Aging mechanisms in amorphous phase-change materials. *Nat. commun.* **6**, 1-8 (2015)
12. T.H. Lee, S.R. Elliott, Chemical Bonding in Chalcogenides: The Concept of Multicenter Hyperbonding. *Adv. Mater.* **32**, 2000340 (2020)]
13. A. Gallo-Bueno, M. Kohout, E. Francisco, A.M. Pendás, Localization and Delocalization in Solids from Electron Distribution Functions, *J. Chem. Theory Comput.* **18**, 4245-4254 (2022)
14. D.A. Keen, M.T.T. Dove, Local structures of amorphous and crystalline phases of silica, SiO₂, by neutron total scattering. *J. Phys.: Condens. Matter* **11**, 9263 (1999)
15. C. Massobrio, A. Pasquarello, Structural properties of amorphous GeSe₂. *J. Phys.: Condens. Matter.* **19**, 415111 (2007)

16. P.S. Salmon, I. Petri, Structure of glassy and liquid GeSe₂. *J. Phys.: Condens. Matter* **15**, S1509 (2003)
17. K. Konstantinou, J. Mavračić, F.C. Mocanu, S.R. Elliott, S. R. Simulation of Phase-Change-Memory and Thermoelectric Materials using Machine-Learned Interatomic Potentials: Sb₂Te₃. *Phys. Status Solidi B* **258**, 2000416 (2021)
18. P. Jónvári *et al.*, Local order in amorphous Ge₂Sb₂Te₅ and Ge₂Sb₂Te₄. *Phys. Rev. B* **77**, 035202 (2008)
19. J.Y. Raty, C. Otjacques, J.P. Gaspard, C. Bichara, C. Amorphous structure and electronic properties of the Ge₁Sb₂Te₄ phase change material. *Solid State Sci.* **12**, 193-198 (2010)
20. L. Guarneri *et al.*, Metavalent bonding in crystalline solids: how does it collapse? *Adv. Mater.* **33**, 2102356 (2021)

